







Motoneuron deafferentation and gliosis occur in association with neuromuscular regressive changes during ageing in mice

Alba Blasco^{1†} , Sílvia Gras^{1†} , Guillem Mòdol-Caballero² , Olga Tarabal¹ , Anna Casanovas¹ , Lúdia Piedrafita¹ , Alejandro Barranco³ , Tapas Das⁴ , Suzette L. Pereira⁴ , Xavier Navarro² , Ricardo Rueda³ , Josep E. Esquerda¹ & Jordi Calderó^{1*}

¹Unitat de Neurobiologia Cel·lular, Departament de Medicina Experimental, Facultat de Medicina, Universitat de Lleida, Institut de Recerca Biomèdica de Lleida (IRBLleida), Lleida, Spain, ²Grup de Neuroplasticitat i Regeneració, Institut de Neurociències, Departament de Biologia Cel·lular, Fisiologia i Immunologia, Universitat Autònoma de Barcelona, CIBERNED, Bellaterra, Spain, ³Abbott Nutrition Research and Development, Granada, Spain, ⁴Abbott Nutrition Research and Development, Columbus, OH, USA

Abstract

Background The cellular mechanisms underlying the age-associated loss of muscle mass and function (sarcopenia) are poorly understood, hampering the development of effective treatment strategies. Here, we performed a detailed characterization of age-related pathophysiological changes in the mouse neuromuscular system.

Methods Young, adult, middle-aged, and old (1, 4, 14, and 24–30 months old, respectively) C57BL/6J mice were used. Motor behavioural and electrophysiological tests and histological and immunocytochemical procedures were carried out to simultaneously analyse structural, molecular, and functional age-related changes in distinct cellular components of the neuromuscular system.

Results Ageing was not accompanied by a significant loss of spinal motoneurons (MNs), although a proportion (~15%) of them in old mice exhibited an abnormally dark appearance. Dark MNs were also observed in adult (~9%) and young (~4%) animals, suggesting that during ageing, some MNs undergo early deleterious changes, which may not lead to MN death. Old MNs were depleted of cholinergic and glutamatergic inputs (~40% and ~45%, respectively, $P < 0.01$), suggestive of age-associated alterations in MN excitability. Prominent microgliosis and astrogliosis [~93% ($P < 0.001$) and ~100% ($P < 0.0001$) increase vs. adults, respectively] were found in old spinal cords, with increased density of pro-inflammatory M1 microglia and A1 astroglia (25-fold and 4-fold increase, respectively, $P < 0.0001$). Ageing resulted in significant reductions in the nerve conduction velocity and the compound muscle action potential amplitude (~30%, $P < 0.05$, vs. adults) in old distal plantar muscles. Compared with adult muscles, old muscles exhibited significantly higher numbers of both denervated and polyinnervated neuromuscular junctions, changes in fibre type composition, higher proportion of fibres showing central nuclei and lipofuscin aggregates, depletion of satellite cells, and augmented expression of different molecules related to development, plasticity, and maintenance of neuromuscular junctions, including calcitonin gene-related peptide, growth associated protein 43, agrin, fibroblast growth factor binding protein 1, and transforming growth factor- β 1. Overall, these alterations occurred at varying degrees in all the muscles analysed, with no correlation between the age-related changes observed and myofiber type composition or muscle topography.

Conclusions Our data provide a global view of age-associated neuromuscular changes in a mouse model of ageing and help to advance understanding of contributing pathways leading to development of sarcopenia.

Keywords Sarcopenia; Ageing; C57BL/6J mice; Motoneurons; Central synapses; Glia; Neuromuscular junction; Skeletal muscle

Received: 3 April 2020; Revised: 5 June 2020; Accepted: 15 June 2020

*Correspondence to: Jordi Calderó, Unitat de Neurobiologia Cel·lular, Departament de Medicina Experimental, Facultat de Medicina, Universitat de Lleida–Institut de Recerca Biomèdica de Lleida, Av. Rovira Roure 80, Lleida 25198, Spain. Phone: +34-973-702440, Email: jordi.caldero@udl.cat

[†]These authors contributed equally to this work.

Introduction

The rise of human life expectancy is a contributing factor of frailty, a common clinical syndrome in the elderly, which is characterized by a state of increased vulnerability to adverse outcomes with subsequent disability and morbidity. Frailty is considered a consequence of a collective age-related decline in the function and reserve of multiple organs, with particular involvement of the neuromuscular, endocrine, and immunological systems.^{1,2} Sarcopenia, defined as the progressive loss of muscle mass, strength, and function, is a key component of physical frailty. Sarcopenia leads to mobility impairments and falls in older adults, negatively affecting their quality of life.³ The prevalence of sarcopenia in people over age 60 years has been reported to be 8–40% depending on the sarcopenia definition used; starting about the age 50, humans lose 1–2% of muscle mass per year, with an annual decline in muscle strength of 1.5% between ages 50 and 60 and of 3% thereafter.^{4,5} Sarcopenia in the elderly has been proposed to have a multifactorial aetiology, which includes chronic inflammation ('inflammageing'), metabolic and endocrine alterations, poor nutrition, mitochondrial dysfunction, oxidative damage, and neurogenic factors.^{6–8} Although notable progress has been made in the understanding of causative factors leading to ageing sarcopenia, the exact cellular and molecular mechanisms responsible for this process still remain elusive. Moreover, there is a remarkable divergence in reported results on the age-related changes observed in distinct components of the neuromuscular system and their contribution to progressive muscle wasting in the elderly. These differences are particularly noticeable when comparing data from different ageing animal models and, even more, when compared with neuromuscular changes reported in human studies. These differences could be due to the fact that many studies focus on specific components of the neuromuscular system rather than a more holistic analysis of the neuromuscular system in its entirety.

Some studies have provided information indicating that an impaired neuromuscular innervation could account for the loss of muscle mass in advanced ages⁹; in line with this, structural changes in both the presynaptic and postsynaptic portions of the neuromuscular junction (NMJ) have been reported to occur with age in both animals and humans.^{10–12} Other studies in aged rodents have reported morphological alterations in motor nerve terminals with increased extent and complexity of their arborization, accompanied by fragmentation of postsynaptic endplates. All these changes appear to reflect continuous cycles of muscle denervation and reinnervation with ageing.¹³ Overall, this process of NMJ remodelling is considered to be a consequence of motoneuron (MN) degeneration with age. Some investigations in humans have reported a significant decrease in the number of MNs in people over 60 years.¹⁴ Similarly, loss of MNs with advancing age has been reported in rodents as well.^{9,15–17} This MN

death could account for the age-associated loss of motor units, particularly of those innervating fast-twitch muscles, and the decrease in muscle power.^{8,18–20} However, the assumption that MN degeneration is the cause of age-related alterations in NMJs is controversial. Thus, some studies performed in murine models have not reported a significant loss of MNs with age.^{21,22} Whatever the case, the fact that age-related alterations in motor nerve terminals are a consequence of an intrinsic skeletal muscle pathology rather than a primary defect in MNs cannot be excluded. In fact, it is well known that muscle fibres play an important role in the maintenance of NMJs.^{23–27} Therefore, a retrograde process ('dying-back') leading to progressive NMJ disruption and MN dysfunction could result from a defect inherent to muscle fibres with the subsequent decline in muscle-derived trophic signals necessary to maintain the integrity and stability of the neuromuscular presynaptic components. This theory is, in part, strengthened by findings indicating that NMJs in humans are remarkably stable throughout the entire adult lifespan,²⁸ suggesting that the structural and functional neuromuscular alterations occurring in the elderly have their main cause in intrinsic muscle deficiencies.

To elucidate the mechanisms leading to age-associated neuromuscular alterations, we undertook a detailed characterization of the pathophysiological changes occurring in the mouse neuromuscular system over the course of ageing. Here, we examined, as a whole, the various distinct cellular components, which shape the neuromuscular system and are essential for proper motor function. We simultaneously analysed structural and molecular changes occurring with age in spinal cord MNs and glia, dorsal root ganglion (DRG) sensory neurons, motor nerves, NMJs, and skeletal muscles of C57BL/6JRj mice. To assess whether age-related changes in muscles are influenced by their regional location (distal or proximal) and specific function, different hindlimb muscles with a distinct position and myofiber type composition were studied. Moreover, to examine *in vivo* the potential age-related changes in muscle innervation, an electrophysiological analysis using quantitative electromyography was performed. A better understanding of the neuromuscular changes occurring with ageing and the pathogenic mechanisms leading to sarcopenia is crucial towards development of effective interventions aimed at prevention and treatment.

Materials and methods

Animals

All animal handling and experimentation procedures were conducted in accordance with the ethical standards laid down in the 1964 Declaration of Helsinki and its later amendments, the European Communities Council Directive 2010/63/EU for

the care and use of laboratory animals, and the norms established by the *Generalitat de Catalunya* [published in the *Diari Oficial de la Generalitat de Catalunya* (DOGC) 2073, 1995]. All experiments were previously evaluated and approved by the Committee for Animal Care and Use of the *Universitat de Lleida* and the Committee for Ethics on Experimental Animal and Human Research of the *Universitat Autònoma de Barcelona*. All efforts were made to minimize suffering and reduce the number of animals in agreement with the European Communities Council Directive (24 November 1986; 86/609/EEC).

C57BL/6JRj mice were supplied by Janvier Labs (Saint Berthevin, France) and were included in four groups of age (young, adult, middle-aged, and old) according to previously defined criteria.²⁹ Briefly, young age was considered at 1–2 months, adult age at 4–10 months, middle age at 10–18 months, and old age at ~19 months and older. The animals used in the present study had the following ages: 1 month (young), 4 months (adult), 14 months (middle-aged), and 24–30 months (old). To avoid potential bias due to gender, only male animals were used in this study. Mice were housed (3 per cage) in the animal care facility of the *Universitat de Lleida* on a 12-h light/dark cycle, having *ad libitum* access to standard laboratory chow and water. According to previous defined criteria,^{30,31} mice displaying tumours, physical abnormalities, and/or evidence of disease were excluded from the study and euthanized by an overdose of pentobarbital (30 mg, intraperitoneally).

Motor behaviour tests

To evaluate the impact of age progression on motor skills, mice were periodically weighed and carefully examined. Open-field (for assessing locomotor activity) and rotarod and grip strength (for assessing motor coordination and balance) tests were subsequently performed every 4 weeks according to previously described guidelines.³² All tests were conducted by the same investigator. Except for open-field test, every mouse was evaluated 3 times with a 15 min recovery period between them; the value obtained in the best test performance was used as the final score. Open-field test was performed by the automated recording of mouse movements using Smart Video Tracking software (v2.5.21, Panlab Harvard Apparatus, Holliston, MA, USA); different parameters such as time, distance, entries in zones, and average speed were measured.

Electrophysiology tests

Nerve conduction tests were performed in adult and old mice. For motor nerve conduction tests, the sciatic nerve was stimulated percutaneously by means of single pulses of

25 μ s duration delivered through a pair of needle electrodes placed at the sciatic notch. The compound muscle action potential (CMAP, M wave) and the H-reflex wave were recorded from tibialis anterior (TA) and plantar interossei (PL) muscles with microneedle electrodes.³³ The H/M ratio was calculated as the quotient of the maximal H wave and maximal M wave amplitude for each recorded muscle. For sensory nerve conduction tests, the recording electrodes are placed near the digital nerves of the fourth toe to record the compound sensory nerve action potential following stimulation of the sciatic nerve as mentioned previously. All potentials were amplified and displayed on a digital oscilloscope (Tektronix 450S, Tektronix, Beaverton, OR, USA) at appropriate settings to measure the amplitude from baseline to the maximal negative peak and the latency from stimulus to the maximal negative peak. To ensure reproducibility, the recording needles were placed under microscope to secure the same placement on all animals guided by anatomical landmarks. During the tests, the mice body temperature was maintained constant between 34°C and 36°C by means of a thermostat heating pad.

We also performed a motor unit number estimation (MUNE) test in the TA muscle, using the same setting as for the motor nerve conduction test. The protocol used was based on the incremental technique.³⁴ Starting from sub-threshold intensity, the sciatic nerve was stimulated with single pulses of gradually increased intensity until the first CMAP response appeared, representing the first motor unit recruited. With the next stimuli, quantal increases in the response were recorded. Increments $>50 \mu$ V were considered as the recruitment of an additional motor unit. The amplitude of a single motor unit was calculated as the mean of more than 15 consistent increases. The estimated number of motor units resulted from the equation: MUNE = CMAP maximal amplitude/mean amplitude of single motor unit action potentials.

Tissue sample preparation, histological analysis, and motoneuron counts

At chosen time points, mice were anaesthetized and transcardially perfused with 4% paraformaldehyde (PFA) in 0.1 M phosphate buffer (PB), pH 7.4. After animal perfusion, spinal cords, L4 DRGs and ventral nerve roots (VRs), and entire hindlimb skeletal muscles were rapidly dissected. Nerve roots were then immersed in 1% PFA and 1% glutaraldehyde in 0.1 M PB at pH 7.4 for 24 h. Muscle samples were processed for histology and further morphometry according to previously described procedures.³⁵ Muscles examined include the extensor digitorum longus (EDL), a fast-twitch muscle involved in the dorsiflexion of the foot and extension of toes during locomotion; the TA, a fast-twitch muscle, which helps with dorsiflexion and inversion of the foot; the soleus (Sol), a

relative slow-twitch muscle in mice, which plays an important function in maintaining the standing posture and is also utilized for plantarflexion during walking; and the gracilis (Gra), a fast-twitch, more proximal muscle, located in the medial side of the thigh, which is mainly involved in adduction of the limb and also assists knee flexion.³⁶

For histology and MN counts, the spinal cords surrounded by their vertebrae were maintained in Bouin's solution for 2 months and embedded in paraffin. Serial transverse sections (14 μm thick), obtained throughout the entire lumbar (L1–L5) segment, were stained with haematoxylin and eosin (H&E). α -MNs, located in the ventral horn, were identified by their size (soma diameter > 20 μm), morphology (multipolar appearance, prominent nucleolus, and abundant Nissl granules in cytoplasm), and topography in Lamina IX of grey matter. MNs were counted blindly on one side of every 10th section, according to previously described criteria.^{37,38} Briefly, only MNs with a large nucleus and a visible clump of nuclear material and a substantial intense basophilic cytoplasm were included in the counts. These stringent criteria make not necessary the use of a correction factor for double counting.³⁷ The number of cells counted was multiplied by 10 to obtain the total number of MNs per ventral horn.

Ventral nerve roots were postfixed in 1% osmium tetroxide and embedded in Embed 812 (Electron Microscopy Sciences, Fort Washington, PA, USA) epoxy resin, following standard procedures. Semithin transversal sections (1 μm thick) were stained with methylene blue and imaged using an Olympus 60x/1.4NA PlanApo oil immersion objective (Olympus) and a DMX 1200 Nikon (Tokyo, Japan) digital camera.

Muscles were cleaned, cleared of the excess of connective tissue, blotted dry, and weighed. After this, muscles were postfixed in 4% PFA in 0.1 M PB (pH 7.4), cryoprotected with 30% sucrose in 0.1 M PB, embedded in tissue freezing medium (Triangle Biomedical Sciences, Durham, NC, USA), and frozen. Cryostat transverse sections (16 μm thick), obtained from the mid-belly of the muscle, were stained with H&E.

Immunocytochemistry and imaging

For immunocytochemical analysis, lumbar spinal cords, L4 DRGs, and skeletal muscles were postfixed by immersion in 4% PFA in 0.1 M PB (pH 7.4), either overnight (for spinal cords and DRGs) or for 2 h (for muscles), and cryoprotected. Tissue samples were embedded in tissue freezing medium and frozen. Longitudinal (16 μm thick for muscles) and transverse (16 μm thick for muscles and 14 μm thick for spinal cords and DRGs) serial cryostat sections were obtained and stored at -80°C .

Tissue sections were sequentially rinsed in phosphate-buffered saline containing 0.1% Triton X-100 for 30 min, blocked in normal goat serum or normal horse serum, and subsequently incubated with the chosen primary

antibody. The primary antibodies used are indicated in *Table 1*.

After incubation with the primary antibody, sections were washed with phosphate-buffered saline and incubated for 1 h at room temperature with the appropriate secondary fluorescent antibodies labelled with one of the following fluorochromes (1:500): Alexa Fluor 488, Alexa Fluor 546 (Molecular Probes, Eugene, OR, USA), Cy3, or Cy5 (Jackson ImmunoResearch Laboratories, West Grove, PA, USA). The spinal cord sections were finally counterstained with blue fluorescent NeuroTrace Nissl staining (1:100; Molecular Probes). Muscle sections were incubated with Alexa Fluor 555-conjugated α -bungarotoxin (α -Bgtx, 1:500; Molecular Probes) to identify postsynaptic acetylcholine receptors. Some sections were also stained with 4',6-diamidino-2-phenylindole dihydrochloride (DAPI, 50 ng/mL; Molecular Probes) for DNA staining. To avoid lipofuscin-like autofluorescence, slides with sections of spinal cord from old mice were treated with the Autofluorescence Eliminator Reagent (Merck, Madrid, Spain), following incubation with the secondary antibodies. Some slides with DRG were stained with fluorescein isothiocyanate (FITC)-conjugated *Bandeiraea simplicifolia* lectin [isolectin B₄ (IB4), 1:25; Sigma-Aldrich, St. Louis, MO, USA].

After washing, slides were coverslipped using an anti-fading medium containing 0.1 M Tris-HCl buffer (pH 8.5), 20% glycerol, 10% Mowiol, and 0.1% 1,4-diazabicyclo[2,2,2]octane. Slides were examined with and Olympus BX51 epifluorescence microscope (Olympus, Hamburg, Germany) equipped with a DP30BW camera or FluoView 500 or FluoView 1000 Olympus laser scanning confocal microscopes. For comparisons, slides from different animals and experimental conditions were processed in parallel for immunocytochemistry and subsequent imaging. The same scanning parameters were used for the acquisition of images corresponding to different experimental groups. For spinal cord immunocytochemical studies, digital images of the entire lumbar region were obtained from every 30th section.

Electron microscopy

Ultrathin sections of L4 VRs embedded in Embed812 were obtained and counterstained with uranyl acetate and lead citrate. Sections were observed in a JEOL JEM 1400 (JEOL, Tokyo, Japan) transmission electron microscope.

Image analysis and morphometry

Image and morphometric examinations were performed on blinded images by two independent investigators. Digital images were analysed with ImageJ software (US National Institutes of Health, Bethesda, MD, USA).

Table 1 Primary antibodies used for immunocytochemistry

Target	Host species	Source/catalogue no.	Dilution
14-3-3	Mouse monoclonal	BD Transduction Laboratories (San Jose, CA)/F46820	1:100
Agrin	Mouse monoclonal	Millipore (Temecula, CA)/MAB5204	1:100
Calcitonin gene-related peptide	Rabbit polyclonal	Sigma-Aldrich (St. Louis, MO)/C8198	1:1000
CD206	Goat polyclonal	R&D Systems (Minneapolis, MN)/AF2535	1:100
Choline acetyltransferase	Goat polyclonal	Millipore/AB144	1:250
Fibroblast growth factor binding protein 1	Rabbit polyclonal	Bioss Antibodies, (Boston, MA)/bs-1768R	1:80
Glial fibrillary acidic protein	Chicken polyclonal	Abcam (Cambridge, UK)/ab4674	1:1000
Growth associated protein 43 (H-100)	Rabbit polyclonal	Santa Cruz Biotechnology (Dallas, TX)/sc-10786	1:50
Ionized calcium-binding adaptor molecule 1	Rabbit polyclonal	Wako Pure Chemical Industries Ltd. (Osaka, Japan)/019-19,741	1:500
Ionized calcium-binding adaptor molecule 1	Goat polyclonal	Abcam/ab5076	1:500
Laminin	Rabbit polyclonal	Abcam/ab30320	1:1000
Mac-2	Rat monoclonal	Cedarlane (Burlington, Canada)/CL8942AP	1:800
Matrix metalloproteinase-9	Goat polyclonal	Sigma-Aldrich/M9570	1:10
Myosin heavy chain I	Mouse monoclonal	Developmental Studies Hybridoma Bank [DSHB] (Iowa City, IA, USA)/A4-840	1:5
Myosin heavy chain IIA	Mouse monoclonal	DSHB/SC-71	1:20
Myosin heavy chain IIB	Mouse monoclonal	DSHB/BF-F3	1:20
Neurofilament 68 KDa	Chicken polyclonal	Abcam/ab72997	1:1000
Paired box protein 7	Mouse monoclonal	R&D Systems/MAB1675	1:50
Parvalbumin	Mouse monoclonal	Swant (Marly, Switzerland)/PV235	1:2000
S100 β	Rabbit polyclonal	Abcam/ab41548	1:3000
Synaptic vesicle protein 2	Mouse monoclonal	DSHB/SV2	1:1000
Transforming growth factor- β 1	Rabbit polyclonal	Abcam/ab92486	1:100
Vesicular acetylcholine transporter	Guinea pig polyclonal	Synaptic Systems (Gottingen, Germany)/#139105	1:500
Vesicular GABA transporter	Guinea pig polyclonal	Synaptic Systems/#131004	1:200
Vesicular glutamate transporter 1	Rabbit polyclonal	Synaptic Systems/#135302	1:1000
Vesicular glutamate transporter 2	Guinea pig polyclonal	Synaptic Systems/#135404	1:200

Myofiber cells counts and size measurements were performed in a single random image per muscle taken from its mid-belly and immunostained for laminin. Myofiber type composition of different muscles was examined in transversal sections immunostained with different isoform-specific anti-myosin heavy chain (I, IIA, and IIB) antibodies (for types 1, 2A, and 2B myofibers, respectively). Images were captured with a digital camera (Olympus DP30BW), and the number of types 1 (slow-twitch), 2A (fast-twitch fatigue-resistant), and 2B (fast-twitch fast-fatigable) myofibers was counted and expressed as a percentage of total myofiber number. The proportion of myofibers showing central nuclei was also counted on images from DAPI-stained sections. The percentage of myofibers showing lipofuscin aggregates and the number and the area of these aggregates were also measured using ImageJ.

The cytoarchitecture of the NMJs was assessed in longitudinal immunostained sections of muscles. Z-stack optical sections (1 μ m thick) were obtained with the confocal microscope and projected to reconstruct NMJs; maximum intensity projections of stacks were created using the microscope software. Three to five sections were examined for each muscle, in which NMJs from different randomly selected visual fields were analysed. NMJ size was measured by determining the area of manually outlined α -Bgtx-labelled

postsynaptic site. Full or partial denervation is considered when the postsynaptic site was not completely apposed by the nerve terminal immunostained for both neurofilament 68 KDa (NF) and synaptic vesicle protein 2, as presynaptic marker. Single or polyinnervation was estimated counting the number of preterminal axons, stained with anti-NF antibody, entering a single postsynaptic site: an NMJ was defined as polyinnervated when it was occupied by two or more axons. Terminal sprouting was quantified by counting the number of NF-stained axonal processes coming from a nerve terminal that escaped from an α -Bgtx-labelled postsynaptic site; the number of sprouts per NMJ counted was referred as a percentage of the total number of NMJs examined per muscle. On the basis of the morphological appearance of the postsynaptic site, the degree of NMJ maturity was classified as plaque, folds, perforations, or pretzel-like (secondary) structure ranging from immature to mature, according to previously described criteria.³⁹ An NMJ was defined as fragmented when its postsynaptic site displayed a discontinued appearance, with five or more acetylcholine receptor (AChR) islands stained with α -Bgtx and/or unusually small and irregular clusters of AChR. Immunostaining for calcitonin gene-related peptide (CGRP), growth associated protein 43 (GAP-43), agrin, fibroblast growth factor binding protein 1

(FGFBP1), and transforming growth factor- β 1 (TGF- β 1) was estimated based on pixel intensity after background subtraction in NMJs, which postsynaptic site was visualized with α -Bgtx; an average of 50 NMJs per muscle was examined to assess the different morphometric parameters and the intensity of immunostaining. Any NMJ that was difficult to examine due to its location and/or orientation was excluded from the analysis. AChR extrasynaptic accumulations were quantified by estimating the number of α -Bgtx labelled spots in muscle sections after synaptic α -Bgtx exclusion; an average of 35 muscle sections from 3–5 animals per condition were analysed.

The analysis of central synapses, CGRP and matrix metalloproteinase-9 (MMP-9) in MNs, and glia in the ventral horn was performed on confocal images taken from every 30th section of the entire lumbar spinal cord. The number and area of vesicular acetylcholine transporter (VAcChT), vesicular glutamate transporter 1 (VGluT1), VGluT 2, and vesicular GABA transporter (VGAT)-immunoreactive synaptic boutons on MN somata were counted and measured by delineating their periphery on the screen; only boutons that were in close contact with MNs displaying a large nucleus and visible nucleolus were included in the counts, and numbers were normalized to the perimeter of MN soma. Levels of immunoreactivity for ionized calcium-binding adaptor molecule (Iba1), Mac-2, CD206, glial fibrillary acidic protein (GFAP), 14-3-3, and S100 β in the spinal cord and those of CGRP and MMP-9 in MNs were quantified by analysing pixel intensity following background subtraction. Spinal cord microglia morphology was quantified in confocal images from Iba1-immunostained sections by using an ImageJ software for skeleton analysis [AnalyzeSkeleton (2D/3D) from <http://imagej.net/AnalyzeSkeleton>]. Analysis was performed according to a previously described procedure.⁴⁰ For this, digital photomicrographs were transformed to 8-bit grayscale and then binarized to obtain a black and white image by means of a formerly established threshold. Every image was manually edited to obtain an image with a continuous set of pixels and gaps between processes belonging to neighbouring cells. The image was then saved, and the plugin AnalyzeSkeleton (2D/3D) was run. The accuracy of skeletonized images was assessed, by creating an overlay of the obtained skeleton with the corresponding original image.

The number and soma area of CGRP, IB4, and parvalbumin (PV)-immunolabelled sensory neurons in the DRGs were measured on digital images.

The number and diameter of healthy and degenerating myelinated axons were determined on $\times 60$ images taken from VR semithin cross sections stained with methylene blue. The images were joined together to obtain a whole picture of an entire nerve root transverse section; the diameter of the myelinated axons was measured by delineating the outer profile of the myelin sheath. Axon diameter and g -ratio measurements were performed on electron micrographs of VRs. ImageJ g -ratio plugin was used to obtain semiautomated

measurement of randomly selected nerve fibres; the axon diameter was divided by the outer diameter of the myelin sheath. At least 100 myelinated axons per mouse (4–5 mice per condition) were measured.

Statistical analysis

Data are reported as mean \pm standard error of the mean. The statistical analysis was performed by either one-way or two-way analysis of variance followed by *post hoc* Bonferroni's test or two-tailed Student's t -test when only two different groups were compared. The level of significance was established at $P \leq 0.05$. GraphPad Prism 6 software was used for statistical analysis and graph presentations of data.

Results

Reduction in the locomotor activity of mice during ageing

As expected, the body weight of animals was different with age. A gradual increase in growth-related weight was observed between 4 and 10 months of age (Supporting Information, *Figure S1A*). However, the older animals (19–28 months of age) had significant lower average weight than the adults (Supporting Information, *Figure S1A*). Moreover, as mice age, a gradual and significant decline in locomotor activity was detected with the open-field test, with this decline being markedly prominent from 24 months onwards (Supporting Information, *Figure S1B* and *C*). In our hands, rotarod and grip strength tests were not suitable for monitoring the age-associated progression of changes in motor skills; several confounds and challenges in the interpretation of results were found with these tests, particularly when performed in young and adult mice: a number of them fell soon after they were placed on either the rod or the wire grid, or refused the tests. This aspect is not unusual in longitudinal assessments or repetitive tests, as those performed in the present study: after test repetitions, the animals end up learning the innocuous consequences of falling.³² Although these mice were excluded from the analysis, we think that data from rotarod and grip strength tests were not reliable enough to be conclusive. For this reason, we preferred to focus in results from open-field test.

Age-related electrophysiological changes

Data from the nerve conduction tests are detailed in *Table 2*. Compared with adult mice, old (24 months) animals exhibited a reduction in conduction velocity, revealed by an increase in the latency time, in both motor and sensory nerves.

Table 2 Results from motor and sensory nerve conduction tests

Parameter	Adult (6 months, <i>n</i> = 10)	Old (24 months, <i>n</i> = 8)
TA Lat (ms)	1.48 ± 0.06	1.54 ± 0.08
TA CMAP (mV)	54.6 ± 1.9	50.7 ± 2.3
SMUA (µV)	1,572 ± 39	1,240 ± 109*
MUNE	42 ± 1.3	38 ± 1.7
PL Lat (ms)	1.89 ± 0.08	2.38 ± 0.17*
PL CMAP (mV)	7.51 ± 0.50	5.24 ± 0.68*
PL H wave Lat (ms)	5.5 ± 0.3	6.7 ± 0.3*
PL H/M ratio (%)	17 ± 3.4	32 ± 4.1*
DgN Lat (ms)	1.27 ± 0.06	1.41 ± 0.05*
DgN CNAP (µV)	31.6 ± 2.8	29.5 ± 2.5
Weight (g)	29.1 ± 0.6	29.5 ± 0.7

CMAP, compound muscle action potential; CNAP, compound nerve action potential; DgN, 4th digital nerve; Lat, latency at the peak of the wave; MUNE, motor unit number estimation; PL, plantar interosseous muscle; SMUA, single motor unit amplitude; TA, tibialis anterior muscle.

Statistical comparisons are made with Student's *t*-test and Sidak-Bonferroni's method for multiple comparisons.

**P* < 0.05 vs. adult group.

Moreover, a decline in the amplitude of the CMAP, which was more evident in the distal PL muscle than in the more proximal TA muscle, was observed. The CMAP amplitude decline was attributable to a slight decrease in both the number and size of motor units (MUNE and single motor unit amplitude, respectively). Interestingly, the sensory CNAP recorded in the toes did not decrease significantly in old mice, suggesting that the motor decline could be accounted, in part, to muscle loss and compressive forces on the foot sole occurring with age.

With regard to the H wave, the electrical counterpart of the spinal stretch reflex, the latency of the H wave in the PL muscle was found to be longer in old mice than in adult mice, although the mean amplitude was similar in both groups. The H/M ratio, indicative of the excitability of the Ia afferent synapses on spinal MNs, was higher in old than in adult mice, likely due to compensatory mechanisms aimed to maintain an adequate muscle reflex response.

Age-related changes in spinal cord motoneurons

On the basis of contradictory data on age-associated MN loss previously reported in humans and rodents,^{9,14–17,21,22,41,42} we decided to re-examine this issue. We first analysed the morphology of lumbar spinal cord MNs in cryostat sections immunolabelled with an antibody against choline acetyltransferase, as an MN marker, and counterstained with fluorescent Nissl for neuron visualization (Figure 1A1–B2). Compared with young MNs, adult MNs showed a slight (although not significant) increase in soma size, consistent with their higher degree of maturity and the increase in the axonal length (Figure 1I). No significant reduction in the average soma size was found in old MNs with respect to adult ones (adult: 536.30 ± 33.03 µm²; old: 508.42 ± 47.22 µm²; *P* > 0.05; Figure 1I), indicating that ageing does not entail an atrophy of spinal cord MNs. We then counted the total

number of apparently healthy MNs present in the whole lumbar spinal cord on serial transverse paraffin sections stained with H&E (Figure 1C–H). We found no significant changes in the total number of lumbar MNs between young, adult, and old mice (Figure 1J), indicating that no overt MN death occurred during ageing. A detailed analysis of H&E-stained spinal cord sections highlighted the presence of some MNs having an abnormal basophilic dark appearance (Figure 1F and H). These 'dark' MNs could be clearly distinguished from commonly lighter stained (apparently healthy) MNs and perhaps represent an injury-related change. Whereas dark MNs were very scarce and found occasionally in young animals, their presence increased with age, so in old animals, the proportion of dark MNs was significantly higher than that in young mice (Figure 1K). In some cases, dark MNs were shrunken and displayed a deformed appearance, which contrasted with other MNs that were hyperstained but maintain a normal architecture. MNs located in the ventral horn of lumbar spinal cord are organized in three major columns (anteromedial, intermediate, and anterolateral), which are the reflection of muscular groups innervated by these MNs. Thus, the anteromedial column MNs innervate axial muscles, whereas MNs located in the intermediate and anterolateral columns innervate proximal and distal hindlimb muscles, respectively. By counting MNs in these three columns independently, we observed that the number of apparently healthy MNs slightly, but not significantly, decreased in the anterolateral column of old mice with respect to adult animals (Figure 1L). We also noticed that the number of dark MNs rose with age in the three MN columns, with this increase being more pronounced in the intermediate column (Figure 1M).

It has been shown that in MN diseases, spinal MNs exhibit differential vulnerability to degeneration.^{39,43,44} In this regard, MNs innervating slow-twitch muscles (slow MNs) exhibit a higher degree of resistance than those innervating fast-twitch muscles (fast MNs). MMP-9 has been reported to be selectively expressed in fast MNs and has been considered as a determinant factor of specific vulnerable neuronal subpopulations.⁴⁵ We wanted to examine whether ageing induced changes in the degree of MN vulnerability to degeneration by analysing MMP-9 expression (a marker of vulnerability) in the spinal cord of young, adult, and old animals. Compared with young mice, the proportion of lumbar spinal cord MNs showing MMP-9-positive immunolabelling was moderately reduced in adult animals (Figure 2A). This reduction was accompanied by a modest, although significant, decrease in the intensity of MMP-9-immunostaining in adult MNs (Figure 2B). No further changes in either the number of MMP-9-positive MNs or MMP-9-staining intensity were noticed in old mice compared with adult mice (Figure 2A and B). In all the ages examined, MNs that were MMP-9 positive displayed a larger size than those which were MMP-9 negative (Figure 2C); this finding is in agreement with previous reports and fits with the statement that MMP-9 is selectively

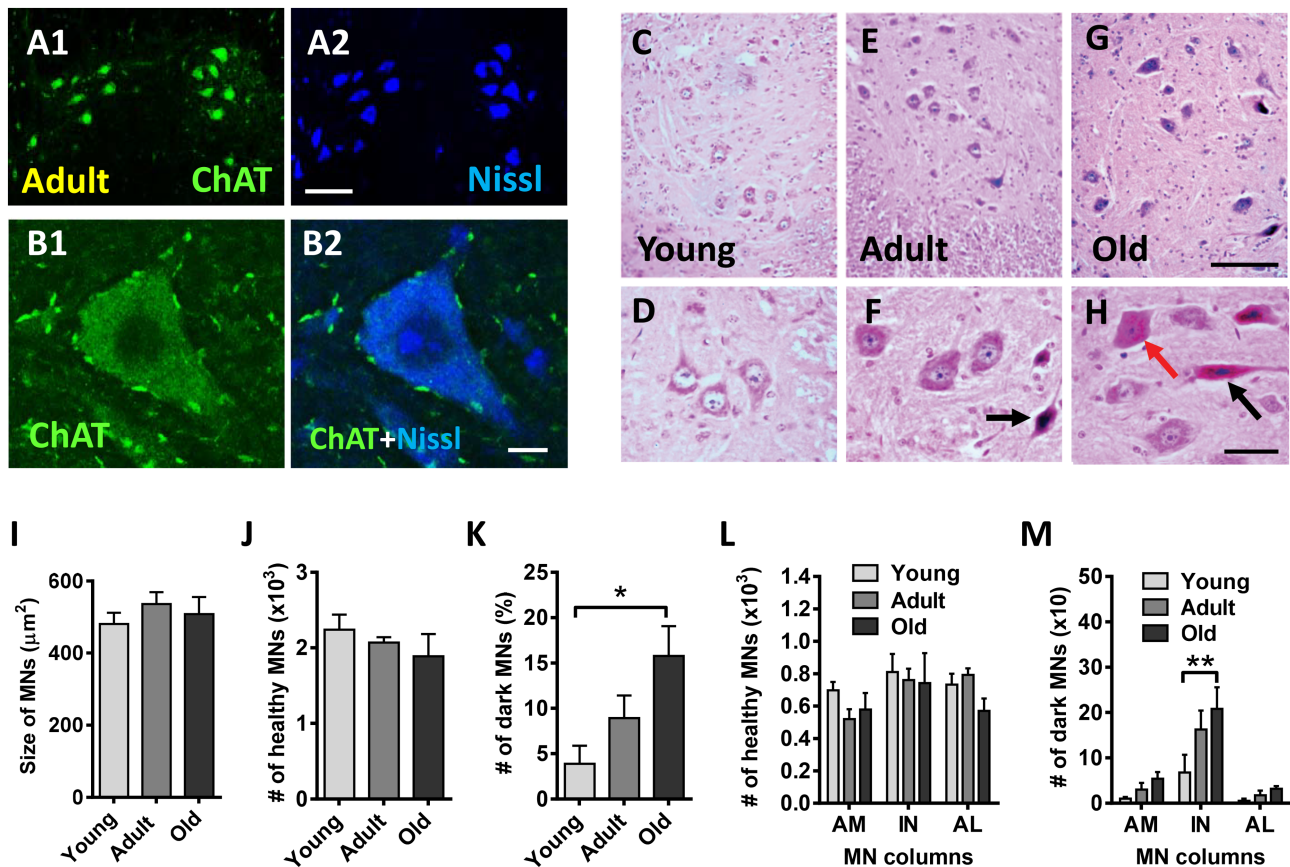


Figure 1 No significant motoneuron (MN) loss occurs in the lumbar spinal cord of mice with ageing. (A1–B2) Representative images of MNs in the spinal cord of adult mice immunolabelled with an antibody anti-choline acetyltransferase (ChAT) (green), as an MN marker, and counterstained with fluorescent Nissl for neuron visualization (blue) as indicated. (C–H) Representative images of haematoxylin and eosin-stained MNs in the lumbar spinal cord of (C and D) young, (E and F) adult, and (G and H) old mice. The appearance of these MNs is shown at a higher magnification in (D, F, and H); black arrows in (F) and (H) indicate dark-stained and shrunken MNs; the red arrow in (H) points to a non-shrunken, hyperchromic, MN. (I) Average size (soma area in μm^2) and (J) number of apparently healthy MNs and (K) proportion of dark MNs (expressed as the percentage of MNs), in the lumbar spinal cord of young, adult, and old mice. (L) Number of healthy and (M) dark MNs in anteromedial (AM), intermediate (IN), and anterolateral (AL) columns of ventral horn. The data in graphs are shown as mean \pm SEM, * $P < 0.05$ and ** $P < 0.01$ (one-way or two-way ANOVA and Bonferroni's *post hoc* test); 4–5 mice per age. Scale bars: (A2) = 100 μm [valid for (A1)]; (B2) = 10 μm [valid for (B1)]; (G) = 100 μm [valid for (C) and (E)]; (H) = 40 μm [valid for (D) and (F)].

expressed in fast, more larger sized, and vulnerable α -MNs.⁴⁵ Moreover, our results suggest that once the degree of vulnerability is achieved in adulthood, no overt changes in MN susceptibility to degeneration occur with age progression.

In MNs, the neuropeptide CGRP is synthesized in the cell body and subsequently transported to nerve terminals where it appears to play a role in the development and maintenance of muscle cells and NMJs.^{46–50} As previously reported by we and others,^{49,51} CGRP was found in subpopulations of spinal cord MNs and, in a particular MN pool, CGRP levels differed between cells, so that some cells exhibited higher contents of this neuropeptide than others. As expected from previous studies (Matteoli *et al.*⁵² and our own observations), compared with young mice, adult animals showed decreased numbers of CGRP-immunostained MNs, with these exhibiting lower levels of immunoreactivity (Figure 2D–F). No significant changes in the number of MNs expressing CGRP were found

in old mice compared with adult animals; old MNs, however, displayed a significant increase in CGRP content compared with adult MNs (Figure 2E and F). Representative immunostaining for MMP-9 and CGRP in young, adult and old MNs is shown in Figure 2G1–I4.

Ageing is accompanied by significant depletion of afferent inputs to motoneurons

We analysed the density of afferent synapses on lumbar spinal cord MNs of old mice compared with adult animals. The number of synaptic boutons on MN somata was quantified after immunostaining with anti-VACHT, VGluT1 and VGluT2, and VGAT antibodies for cholinergic (C-boutons), glutamatergic excitatory, and GABAergic inhibitory synapses, respectively (Figure 3C1–D2, G1–H2, K1–L2, and O1–P2). We

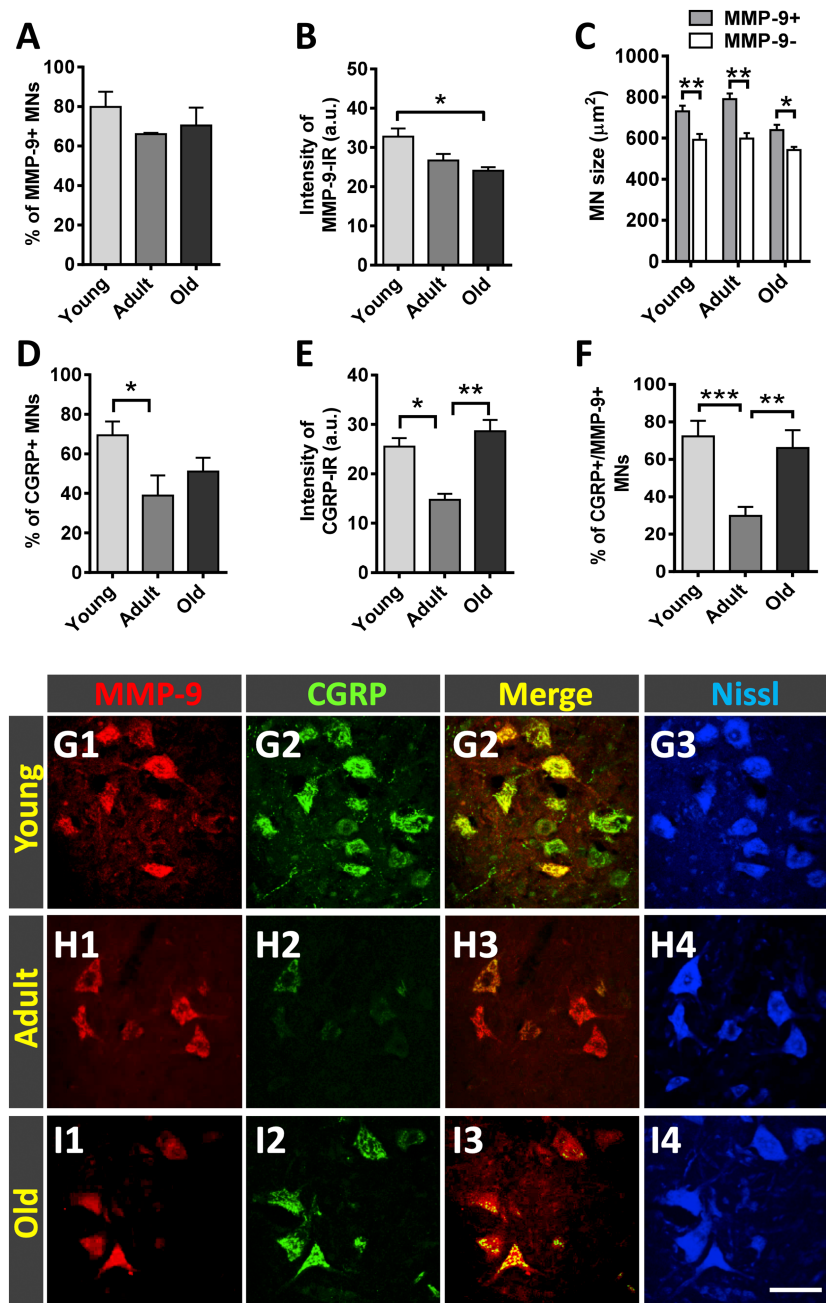


Figure 2 Matrix metalloproteinase 9 (MMP-9) and calcitonin gene-related peptide (CGRP) immunoreactivity in lumbar spinal cord motoneurons (MNs) of young, adult, and old mice; MMP-9 immunostaining is used as a marker of MN vulnerability. (A) Proportion of MNs displaying positive MMP-9-immunoreactivity (IR); the average intensity of the latter is shown in (B). (C) Size (in μm^2) of MN somata exhibiting either positive or negative MMP-9 immunostaining. Age-related changes in the proportion of MNs showing (D) CGRP positivity and (E) in the immunoreaction (IR) intensity in these MNs. (F) Percentage of MNs displaying both CGRP and MMP-9 immunostaining. (G1–I4) Representative images taken from spinal cord sections double immunolabelled for MMP-9 (red) and CGRP (green) and counterstained with fluorescent Nissl staining (blue; for MN visualization). Data in the graphs are expressed as the mean \pm SEM, * $P < 0.05$, ** $P < 0.01$, and *** $P < 0.001$ vs. adult (one-way ANOVA and Bonferroni *post hoc* test); $n = 4$ –6 animals per age; 50 MNs per animal were analysed. Scale bar: (I4) = 60 μm [valid for (G1–I3)].

found that compared with adult MNs, old MNs exhibited a significant decrease in the density of both C-boutons and glutamatergic afferent terminals on cell bodies [$\sim 40\%$ (VACHT), 45% (VGLuT1), and 43% (VGLuT2) decrease] (Figure 3A, B, E,

F, I, and J). No differences in the number of GABAergic synapses were observed between old and adult MNs, although a significant reduction ($\sim 20\%$) in the size of this type of inhibitory afferents was noticed on MNs of old animals (Figure

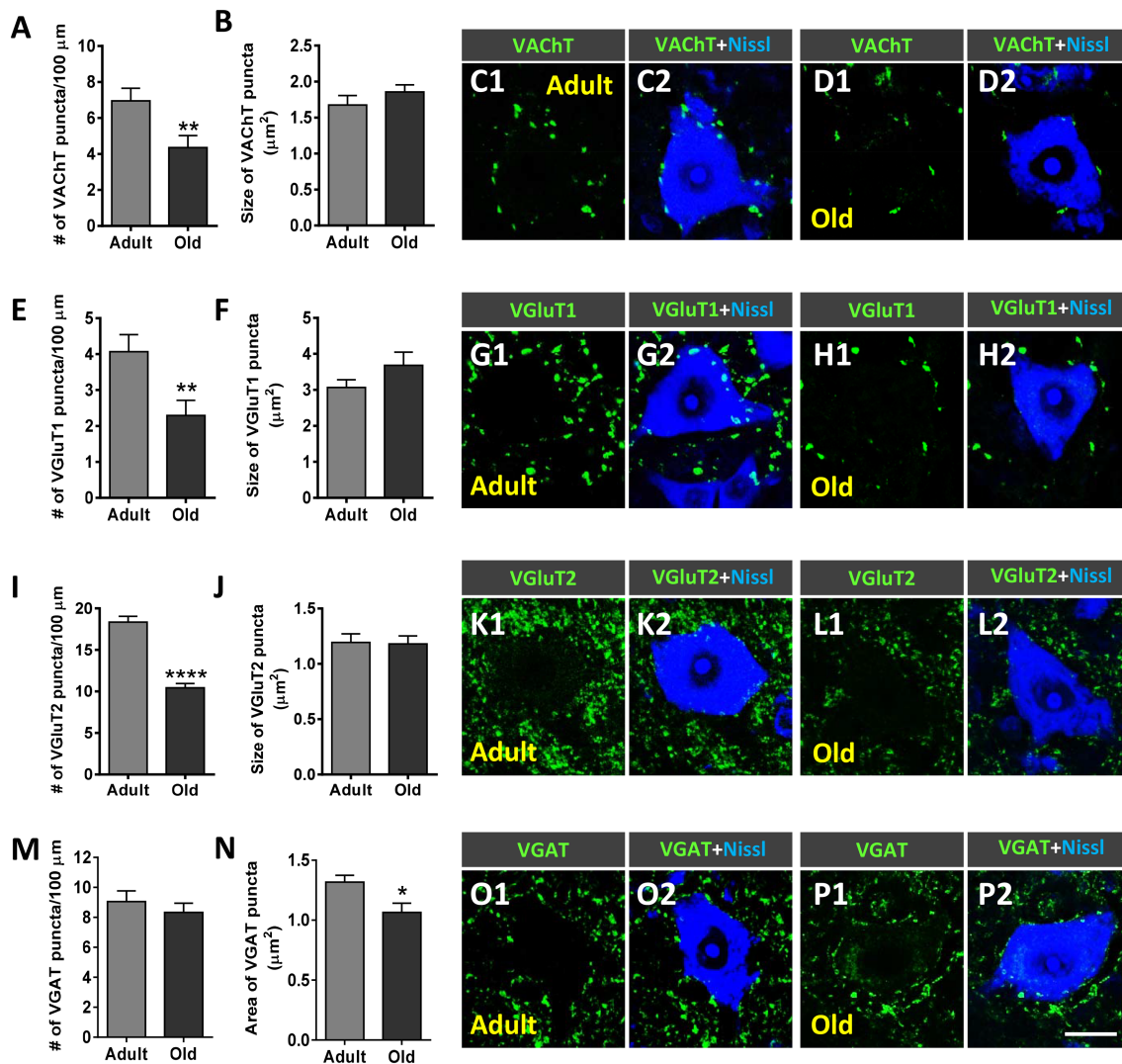


Figure 3 Age-related changes in synaptic inputs to lumbar spinal cord motoneurons (MNs). (A–P2) Sections were immunostained to identify cholinergic [vesicular acetylcholine transporter (VChT)], glutamatergic [vesicular glutamate transporter 1 (VGlut1) and vesicular glutamate transporter 2 (VGlut2)], and GABAergic [vesicular GABA transporter (VGAT)] afferent synapses (green) and counterstained with fluorescent Nissl staining (blue) to visualize MN cell bodies. Graphs show the average density [(A, E, I, and M) number of puncta per 100 μm soma perimeter and (B, F, J, and N) size (in μm²) of the different types of afferent terminals analysed. Representative confocal micrographs of (C1–D2) VChT, (G1–H2) VGlut1, (K1–L2) VGlut2, and (O1–P2) VGAT terminals contacting (C1–C2, G1–G2, K1–K2, and O1–O2) adult and (D1–D2, H1–H2, L1–L2, and P1–P2) old MNs are shown. Data in the graphs are expressed as the mean ± SEM, **P* < 0.05, ***P* < 0.01, and *****P* < 0.0001 vs. adult (Student’s *t*-test); 50–60 MNs were analysed per animal (4–6 animals per age group). Scale bar in (P2) = 20 μm [valid for (C1–D2, G1–H2, K1–L2, and O1–P1)].

3M and N). These results indicate that ageing results in a marked loss of central synapses, mainly involving cholinergic and glutamatergic inputs to MNs.

Gliosis occurs in spinal cord during ageing

Activation of glial cells in the ventral horn of spinal cord has been described to occur in different motoneuronal pathologies including MN diseases and peripheral nerve injury.^{53–57} To explore whether glial activation also occurs in the aged

spinal cord, microglia and astroglia were analysed after immunolabelling for Iba1 and GFAP, respectively (Figure 4A–F2). Compared with adult mice, old animals exhibited significantly higher levels of both Iba1 and GFAP immunoreactivity [~93% and ~100% increase (*P* < 0.001 and *P* < 0.0001), respectively] in the ventral horn of spinal cords (Figure 4A and D), reflecting an increased density of microglial and astroglial profiles. This indicates that prominent microgliosis and astrogliosis occur around aged MNs. The degree of ramification and complexity of microglia was quantified by using a skeleton analysis procedure,⁴⁰ which measures

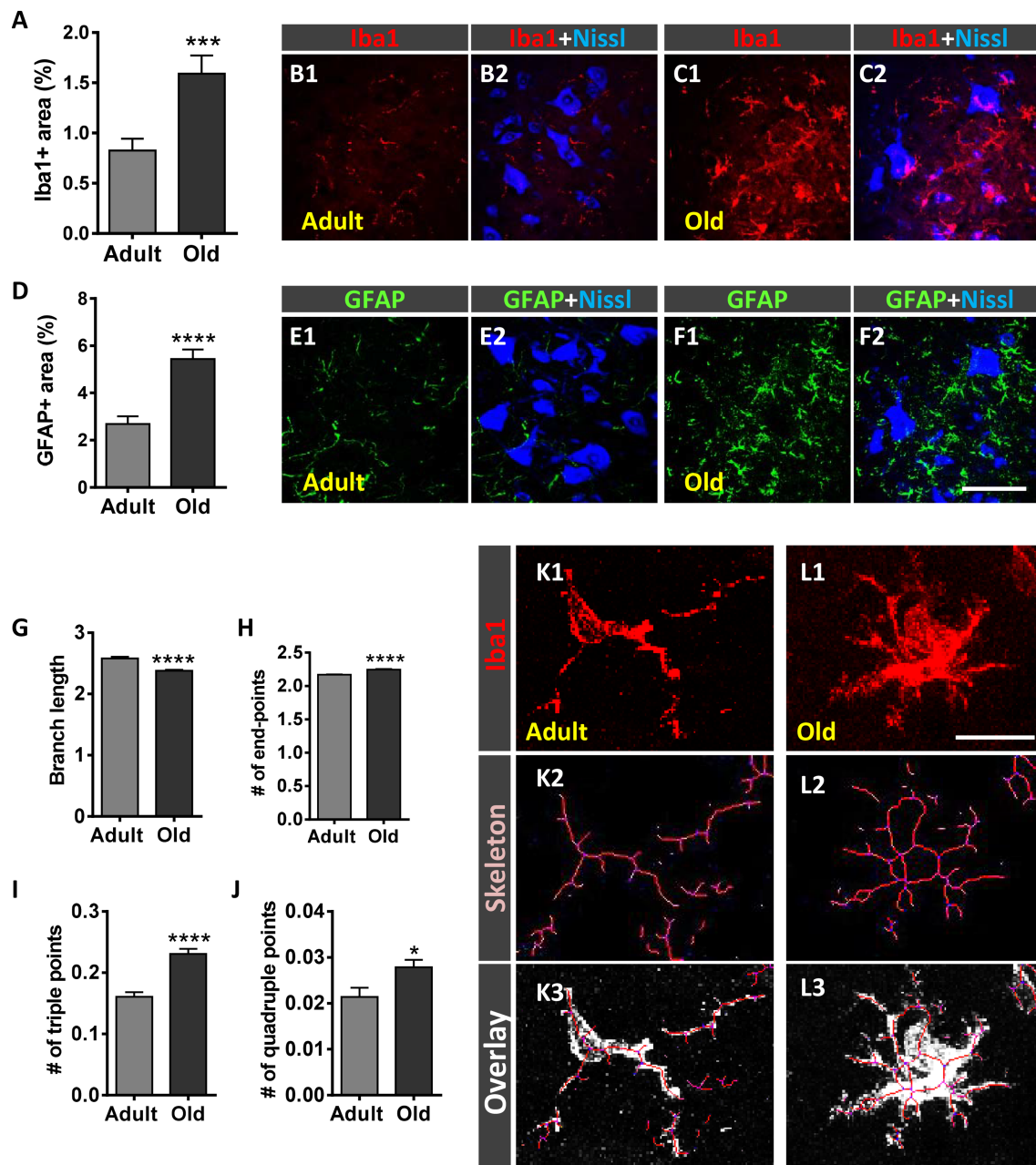


Figure 4 Ageing is accompanied by prominent microgliosis and astrogliosis in the spinal cord. (A–F2) Serial sections of lumbar spinal cord were immunostained to visualize Iba1 and GFAP, for microglia and astroglia, respectively. Quantification of (A) ionized calcium-binding adaptor molecule 1 (Iba1)-positive microglia and (D) glial fibrillary acidic protein (GFAP)-positive astroglia expressed as the percentage of the ventral horn area occupied by Iba1-positive and GFAP-positive profiles. Representative confocal micrographs showing (B1–C2) Iba1 (red) and (E1–F2) GFAP (green) staining in the ventral horn spinal cord of (B1–B2 and E1–E2) adult and (C1–C2 and F1–F2) old mice; fluorescent Nissl staining (blue) was used for motoneuron visualization. (G–L3) Quantification of changes in microglial morphology by using a skeleton analysis procedure (see Materials and Methods section). The average (G) branch length, (H) number of endpoints, and (I) of triple and (J) quadruple points are shown. Representative images showing (K1 and L1) Iba1-stained profiles, (K2 and L2) the skeletonized images, and (K3 and L3) the overlay of the skeleton and the original image of microglia in (K1–K3) adult and (L1–L3) old mice. Data in the graphs are expressed as the mean \pm SEM; the spinal cord of four animals per age group was used for analysis; a total of 40–45 sections (in A and D) and 7,000–12,000 cells (in G–J) per age were examined. * $P < 0.05$, *** $P < 0.001$, and **** $P < 0.0001$ vs. adult (Student's *t*-test). Scale bar: In (F2) = 30 μ m [valid for (B1–C2) and (E1–F1)]; in (L1) = 20 μ m [valid for (K1)].

different parameters of microglia morphology in an entire region of ventral horn (Figure 4G–L3). Compared with adult microglia, those of old mice displayed reduced lengths of

processes and increased number of endpoints in association with significant greater amounts of branches, as indicated by the increased numbers of triple and quadruple points

quantified (Figure 4G–J). These results indicated that with ageing, gliosis involves structural changes in microglia, which become more ramified and complex.

When activated, microglia and astroglia can attain one of two opposing maturation phenotypes: M1 and M2 for microglia and A1 and A2 for astroglia.^{53,58} Whereas M1 and A1 phenotypes have been related to inflammation and degeneration, the M2 and A2 phenotypes have been associated with anti-inflammatory and regenerative processes. To examine which type of microglial and astroglial phenotype is activated in the spinal cord as a consequence of age-related reactive gliosis, Iba1 and GFAP immunocytochemistry was combined with either Mac-2 or CD206 (for M1 or M2 microglia) and 14-3-3 or S100 β (for A1 or A2 astroglia) immunolabelling, respectively^{59–62} (Figure 5A–T). Compared with spinal cords of adult mice, those of old animals exhibited a prominent increase in the density of harmful M1 (Mac-2-positive) profiles and a modest reduction in M2 (CD206-positive) microglia (Figure 5A–D and I1–N). Similarly, the density of A1 (14-3-3-immunostained) astroglia was found to be significantly higher in spinal cords of old mice compared with adult mice (Figure 5E, F, and O1–Q). Although S100 β -immunoreactivity (for A2 phenotype) only showed a moderate, non-significant, decrease around old MNs, the proportion of astroglia that stained positive for both GFAP and S100 β was significantly reduced in old mice compared with adult animals (Figure 5G–H and R1–T). Overall, these findings indicate that age-associated reactive gliosis implies an imbalance in M1/M2 and A1/A2 phenotypes, leading to a polarization to harmful activated M1 and A1 states.

Early degenerative changes in motor nerves during ageing

Ventral nerve roots, which are only formed by the most proximal part of motor axons, were examined to assess their potential structural alterations over the age process. We found that compared with L4 VRs of adult animals, those of middle-aged mice exhibited significantly higher numbers of myelinated axons (Figure 6A). The average axonal diameter (including the myelin sheath) of middle-aged VRs was significantly greater than that of adult VRs (Figure 6B and C). In addition, there was a significant increase in the proportion of degenerating axons in middle-aged VRs compared with adult VRs (Figure 6D, H, and I). Middle-aged VRs had a high number of axons whose myelin sheath structure exhibited focal disruption and, often, protruded into the axonal compartment to ultimately form myelin spheroidal inclusions (Figure 6E, H, and I); these inclusions, having the appearance of myelin-like multilaminar balls, were only occasionally seen in VRs from adult mice and had a similar morphology to that observed during Wallerian degeneration.⁶³ It was not unusual to see myelin debris engulfed by macrophages in middle-aged

VRs. Interestingly, compared with adults, there was an increase in the proportion of small myelinated axons in middle-aged VRs, but this did not reach statistical significance (Figure 6F). In middle-aged VRs, these small axons were usually seen clustered, contrasting with their homogeneous distribution in adult VRs (Figure 6G, H, and I). Clustered small myelinated axons could represent newly formed, still immature, nerve branches, which originate by sprouting from healthy motor axons. These results suggest that early in the ageing process, some motor axons undergo degeneration, and this is accompanied by the reactive generation of new nerve fibres, in an attempt to replace those previously damaged. *G*-ratio analysis allowed us to assess the relationship between axon diameter and myelin thickness. Axon diameter, by delineating the periphery of axon under the myelin sheath, was found to be significantly longer in middle-aged VRs than in those of adult VRs, suggesting that a certain degree of motor axon swelling occurs during ageing (Figure 6J–N). In addition, the thickness of axon myelin was significantly decreased in middle-aged VRs compared with adult VRs, as indicated by the higher *g*-ratio average values found in axons (*g*-ratios: adult age = 0.57 ± 0.12 and middle age = 0.61 ± 0.01 ; $n = 105$ – 285 and 100 – 180 axons per animal, four and five animals, respectively, $P < 0.05$). As shown in the scatter plot of Figure 6N, motor axons of middle-aged mice that were larger corresponded to those with higher *g*-ratios, indicating a thinner myelin sheath. The ultrastructural appearance of middle-aged motor axons at different stages of degeneration is shown in Figure 6O–Q.

Ageing is accompanied by alterations in dorsal root ganglion sensory neurons

To ascertain whether ageing also affects to sensory neurons, L4 DRGs of adult and old mice were examined. DRG sections were processed for immunocytochemistry with antibodies against CGRP and PV and also stained with IB4 lectin (Supporting Information, Figure S2A–O2). These are specific markers for different DRG neuronal subpopulations: CGRP is present in peptidergic, small and medium-sized sensory nociceptive neurons; IB4 stains nonpeptidergic, small-sized sensory nociceptive neurons; and PV is present in large sensory proprioceptive neurons innervating muscle spindles.^{64–66} Compared with the DRGs of adults, old DRGs showed a higher proportion of CGRP-positive, IB4-positive, and PV-positive neurons (Supporting Information, Figure S2A, F, and K). In DRGs of old mice, all these neuronal populations exhibited a significantly smaller soma size compared with those of adult animals (Supporting Information, Figure S2B, C, G, H, L, and M). These data suggest that ageing promotes significant changes in the expression of CGRP, IB4, and PV in sensory DRG neurons, which are accompanied by a marked atrophy of both proprioceptive and nociceptive neurons.

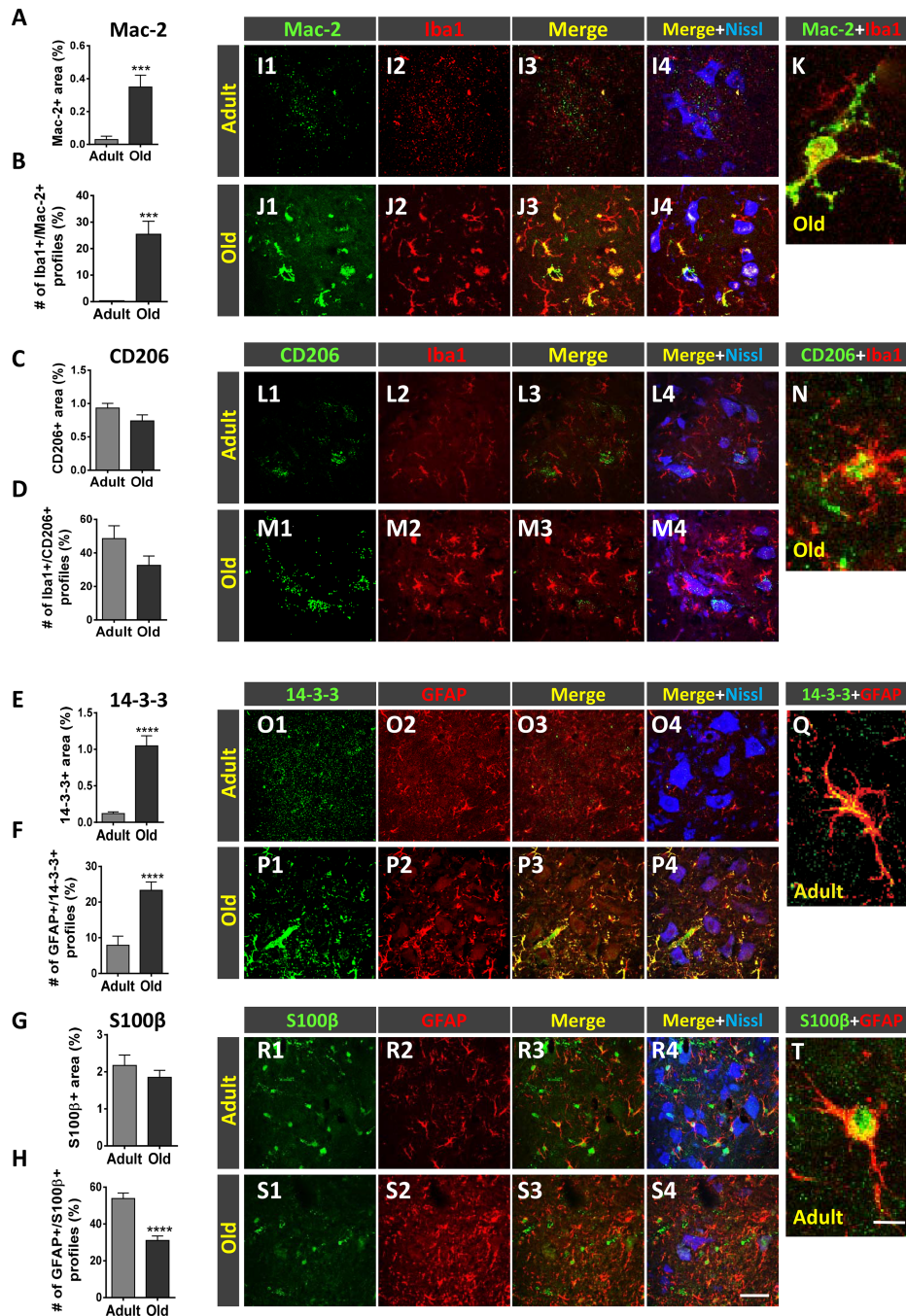


Figure 5 Age-related changes in the phenotype of spinal cord microglia and astroglia. (A–J) Serial sections of lumbar spinal cord of adult and old mice were double immunostained for ionized calcium-binding adaptor molecule 1 (Iba1) and either (M1) Mac-2 or (M2) CD206 microglia, and glial fibrillary acidic protein (GFAP) and either (A1) 14-3-3 or (A2) S100β astroglia. Quantification of (A and C) Mac-2-positive and CD206-positive profiles surrounding motoneurons (MNs), based on the ventral horn area occupied by these immunostained profiles; the proportion of microglial profiles expressing both Iba1 and either Mac-2 or CD206 is shown in (B) and (D), respectively. Quantification of (E and G) 14-3-3-positive and S100β-positive profiles surrounding MNs based on the ventral horn area occupied by these immunostained profiles; the proportion of astroglial profiles expressing both GFAP and either 14-3-3 or S100β is shown in (F) and (H), respectively. Representative confocal micrographs used for data analysis showing (I1–K) Mac-2, (L1–N) CD206, (O1–Q) 14-3-3, and (R1–T) S100β (all in green); microglial and astroglial markers were combined with Iba1 and GFAP, respectively (both in red), and fluorescent Nissl staining (blue) for MN visualization. Higher magnification images of Iba1-positive microglial profiles also expressing either (K) Mac-2 or (N) CD206 and GFAP-positive astroglial profiles also expressing either (Q) 14-3-3 or (T) S100β in the ventral horn of adult spinal cords are shown. Data in the graphs are expressed as the mean \pm SEM; the spinal cord of four animals per age group was used for analysis; a total of 40–45 sections per age were examined. *** $P < 0.001$ and **** $P < 0.0001$ vs. adult (Student's *t*-test). Scale bars: In (S) = 50 μ m [valid for (I1–J4), (L1–M4), (O1–P4), and (R1–S4)] and in (T) = 10 μ m [valid for (K, N, and Q)].

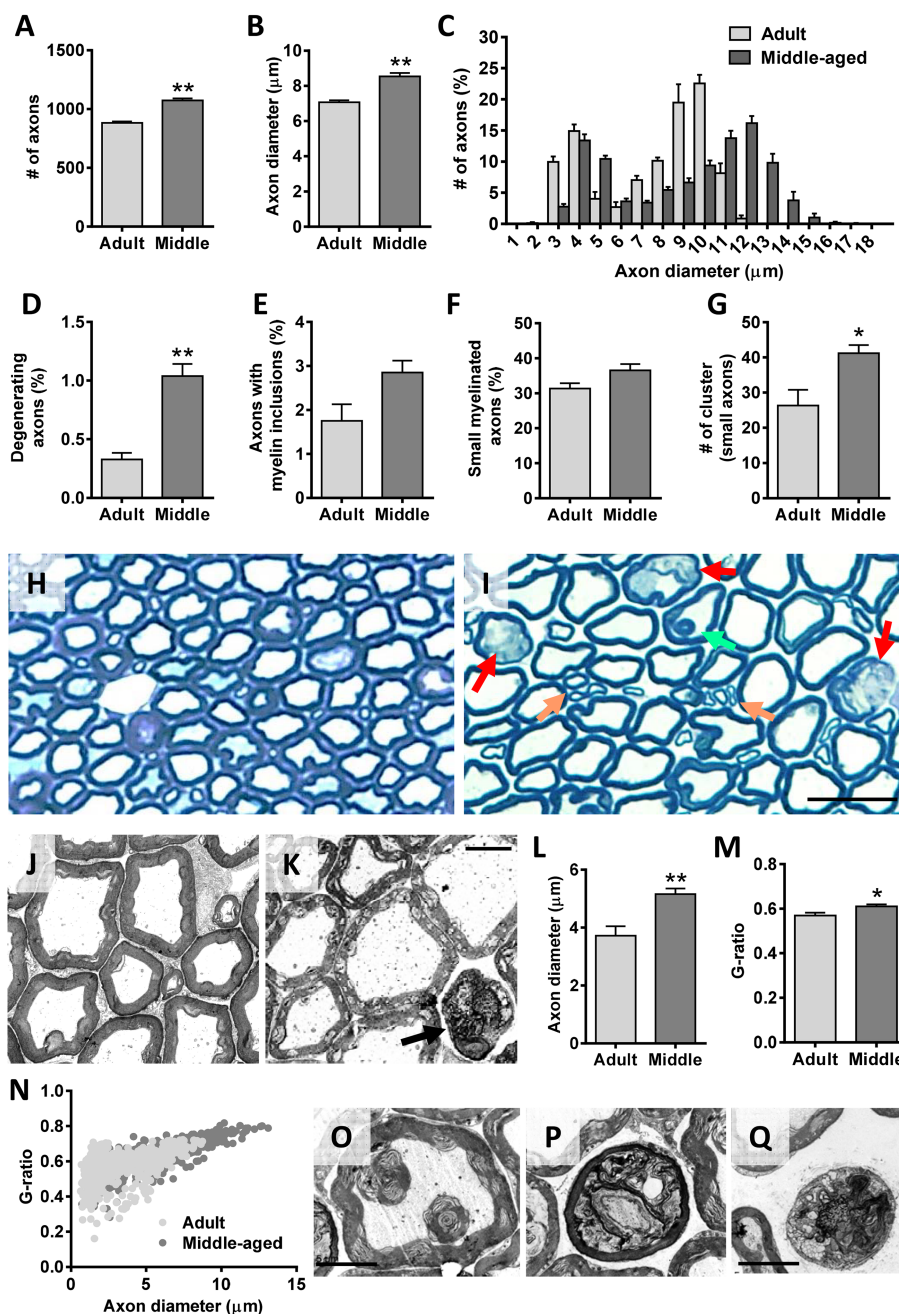


Figure 6 Age-related changes in motor axons of mice. The analysis was performed in L4 ventral roots (VRs) of adult and middle-aged (middle) animals. (A) Number and (B) diameter of VR myelinated axons. (C) Relative frequency of myelinated axon diameter (in μm); note in adult VRs the bimodal profile indicative of axons originating from α-motoneurons (large axons) and γ-motoneurons (small axons). Proportion of axons showing a (D) degenerating appearance, (E) some myelin inclusions, and (F) a small (≤6 μm) diameter; the number of small axon clusters (≥3 axons) in adult and middle-aged VRs are shown in (G). Representative images of methylene blue-stained semithin cross sections of (H) adult and (I) middle-aged VRs used for axon analysis; in (I), arrows indicate degenerating axons (red), a myelin inclusion inside an axon (green), and clusters of small axons (orange). Electron micrographs of (J) adult and (K) middle-aged VRs; note in (K) the distended appearance of some axons and the subtle changes in myelin structure seen in middle-aged motor axons; arrow in (K) points out a degenerating axon. (L) Diameter (in μm) of motor axons, showing a significant increase in axon size of middle-aged animals; the measurements were performed by delineating the axon periphery underneath the myelin sheath. Quantification of myelin thickness by (M) g-ratio analysis and (N) scatter plot depicting (N) g-ratios in relation to axon diameter in VRs; all the measurements in (L–N) were performed on electron micrographs taken from ultrathin cross sections of VRs at comparable levels. Representative electron micrographs of middle-aged VRs showing in (O) a focal disorganization of myelin sheath resulting in two multilamellar myelin balls located inside a motor axon and in (P) and (Q) motor axons in different stages of degeneration. Data in the graphs are expressed as the mean ± SEM, *P < 0.05 and **P < 0.01 vs. adult; n = 4 adult and 5 middle-aged VRs of different animals. Scale bars: In (I) = 25 μm [valid for (H)], (K) = 5 μm [valid for (J)], and (Q) = 5 μm [valid for (O and P)].

Structural and molecular changes in neuromuscular junctions of hindlimb muscles during ageing

The morphology and innervation of NMJs in TA, Sol, EDL, and Gra muscles were examined following double immunostaining for NF and synaptic vesicle protein 2 (for visualization of presynaptic nerve terminals) combined with α -Bgtx (for identification of postsynaptic sites). In adult muscles, both presynaptic and postsynaptic elements displayed a well-organized appearance, with smooth and continuous nerve terminals entering in endplates, the latter showing the 'pretzel-like' pattern characteristic of mature, 'healthy' NMJs; postsynaptic membranes exhibited numerous folds where α -Bgtx-labelled AChRs were concentrated. In contrast, NMJs of old muscles displayed structural alterations, which are consistent with previous reports^{11,22,67–69}: whereas some NMJs appeared partially or fully denervated (*Figure 7A* and F1–H2), a high proportion of innervated NMJs had overt signs of polyinnervation (*Figure 7B*, I1, and I2); moreover, many nerve terminals displayed a more complex branching and sprouting (*Figure 7E*, J1, and J2). Motor endplates of old muscles were also altered, showing increased size and fragmented appearance (*Figure 7C* and D). Endplate denervation was frequently associated with many small spots of clustered AChRs scattered along the myofibers (*Figure 7K–N*). These spots concomitantly displayed a faint positive signal for presynaptic markers, indicative of a reactive neoformation of neuromuscular synaptic contacts (*Figure 7O* and P1–P4). We observed some variations in these changes between muscle types studied: in old mice, the proportion of denervated NMJs was much lower in TA muscles than other muscle types (*Figure 7A*); moreover, TA muscles showed more polyinnervated NMJs than Sol and Gra muscles, with no obvious signs of polyinnervation in EDL muscles of old mice (*Figure 7D*).

We and others have previously reported that during NMJ development, motor nerve terminals initially contain high levels of CGRP, which markedly decreases in mature NMJs; nevertheless, CGRP is up-regulated in NMJs during conditions of reinnervation and nerve sprouting.^{47,50,52,70} Consistent with this, levels of CGRP in NMJs was very low in all adult muscles examined compared with their young counterparts (*Figure 8C1–C3* and B1–B3). Conversely, a significant increase in CGRP immunoreactivity was seen in NMJs of old muscles, this augment being particularly prominent in the Gra muscle (*Figure 8A* and F1–G3).

GAP-43 is a protein present in virtually all neurons during axonal growth, being particularly abundant in axonal growth cones (reviewed in Holahan⁷¹). It has been found that in the neuromuscular system, GAP-43 is down-regulated in MNs at the onset of synapse elimination in a process that is regulated by muscle activity.⁷² Consequently, mature MNs and their corresponding nerve terminals exhibit low levels

of GAP-43. In our study, adult muscles showed very low levels of GAP-43 compared with their young counterparts (*Figure 9B1–B3* and C1–C3). The levels of this protein, however, were significantly increased in the NMJs of old muscles (*Figure 9A* and D1–D3).

Agrin is a protein synthesized in the MN cell body and axonally transported to the nerve terminal where once released concentrates at the synaptic basal lamina to play a crucial role in the process of NMJ formation and maintenance.^{73–76} We analysed then whether agrin content in NMJs was altered in old muscles and found that NMJs of young and adult muscles displayed low levels of agrin (*Figure 9F1–F3* and G1–G3). In comparison, NMJs of all muscles examined from old mice, with the exception of Gra, exhibited a significant increase in agrin expression (*Figure 9E* and H1–H3).

We next examined the expression levels of FGFBP1 and TGF- β 1 in muscles of adult and old mice. FGFBP1 is a secreted protein that binds fibroblast growth factor proteins present at the extracellular matrix enhancing its biological activity.⁷⁷ FGFBP1 has been reported to be transcribed in muscle fibres, where it appears to have a role in regenerating injured NMJs.⁷⁸ On the other hand, TGF- β 1 has been shown to regulate FGFBP1 expression in cultured myotubes.⁷⁹ We found that all the examined muscles from young mice expressed both FGFBP1 and TGF- β 1. Although a diffuse and discrete immunofluorescence was seen along the muscle fibres, both proteins were mainly concentrated at the NMJs (not shown). However, the expression levels of FGFBP1 and TGF- β 1 changed with age. Muscles of adult mice exhibited lower content of both proteins compared with that of young animals. Moreover, compared with adult muscles, old muscles displayed an increased expression of FGFBP1 and TGF- β 1, showing a pattern of immunoreactivity mostly restricted to the synaptic region of muscle (*Figure 10A*, B, and C1–F3). Although both proteins were mainly detected within the postsynaptic α -Bgtx-stained area, some immunolabelling was also seen outside of this region, suggesting that FGFBP1 and TGF- β 1 are in part located in the extracellular matrix around the NMJ.

Age-related changes in hindlimb skeletal muscles

Aged-related changes in skeletal muscles have been reported in some murine models at histological and electrophysiological levels^{68,80–84} (Hunter *et al.*⁸⁵ and McKinnon *et al.*,⁸⁶ as reviews). We examined the degree of histopathological alterations in different mouse muscles to assess the extent by which muscular changes could account for the impaired motor performance observed in old animals. Because muscle denervation is typically associated with muscle atrophy, we determined the wet weight, as an indicator of muscle mass, and the cross-sectional area of muscles. Wet weights of adult and old muscles did not exhibit significant differences, although some reductions in the weight of Sol and EDL muscles

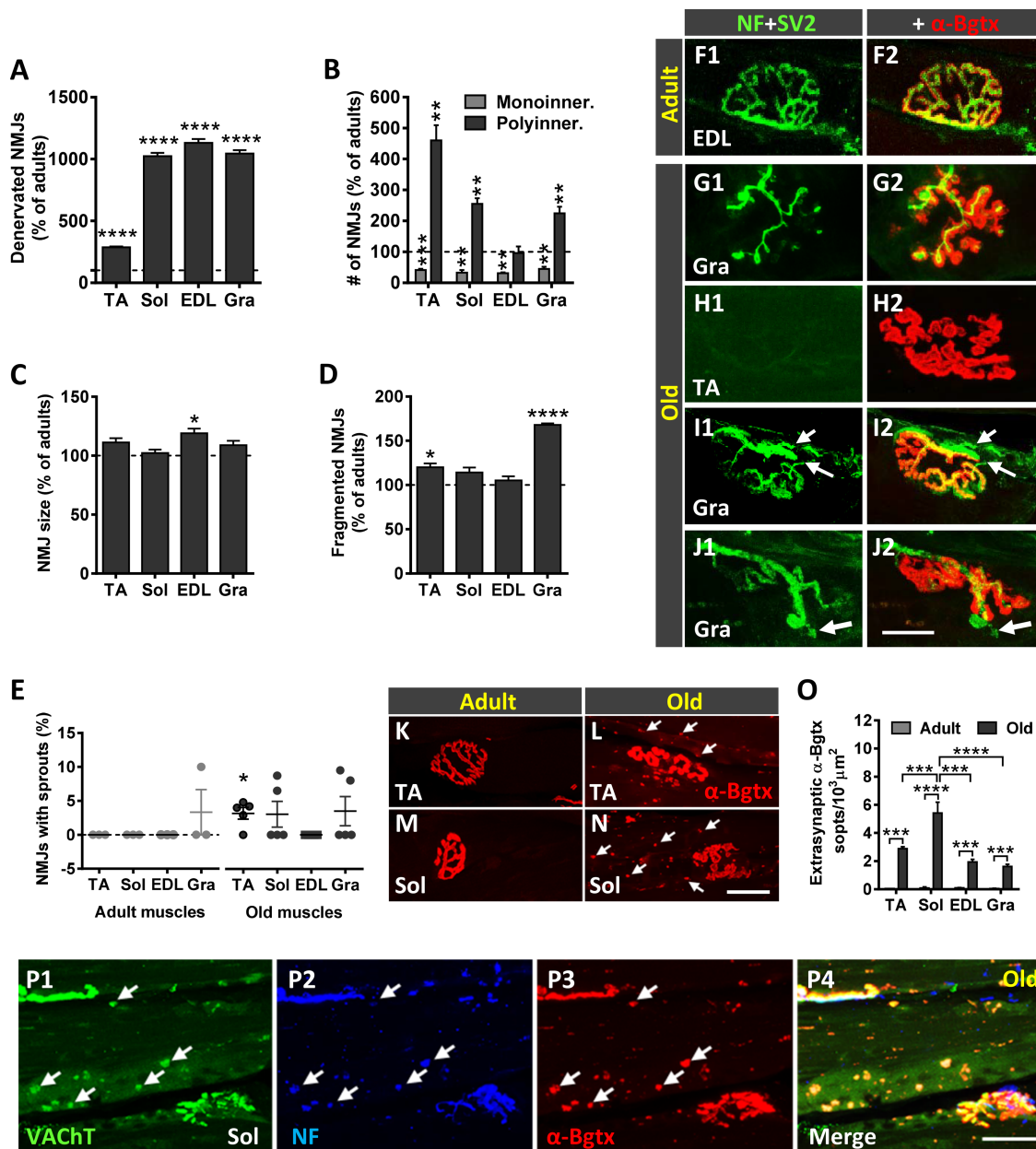


Figure 7 Age-related changes in neuromuscular junctions (NMJs). Proportion of (A) denervated and of (B) monoinnervated and polyinnervated NMJs in muscles of old mice. Changes in (C) NMJ size and (D) number of fragmented endplates in old muscles. All graphs show values as a percentage of change compared with adult muscles; 50–100 NMJs per muscle from four adult and five old mice were analysed. (E) Percentage of NMJs exhibiting terminal axonal sprouts in the muscles of adult and old mice; each point represents the percentage of sprouts found in 25–30 NMJs per muscle from four adult and five old mice. Data in all graphs are expressed as the mean ± SEM, **P* < 0.05, ***P* < 0.01, ****P* < 0.001, and *****P* < 0.0001 vs. adult (one-way ANOVA and *post hoc* Bonferroni’s test). Maximal projections of confocal stacks of NMJs from (F1 and F2) adult and (H1–J2) old muscles, as indicated in panels. Muscle sections were stained with antibodies against neurofilament 68 kDa (NF) and synaptic vesicle protein 2 (SV2) (green) for pre-synaptic nerve terminals and α-bungarotoxin (α-Bgtx) (red) for postsynaptic acetylcholine receptor (AChR). Microphotographs in (G1–J2) correspond to representative old NMJs displaying different structural changes: (G1 and G2) partial innervation, (H1 and H2) denervation, (I1 and I2, arrows) polyinnervation, and (J1 and J2, arrow) terminal sprouting, most of these showing signs of endplate fragmentation; compare with the typical appearance of an innervated adult NMJ in (F1 and F2). Representative images of α-Bgtx-stained (red) endplates in the (K and L) tibialis anterior (TA) and (M and N) soleus (Sol) muscles from adult and old mice; arrows in (L and N) point to patches of AChRs scattered along the myofibers. (O) Density (number per 1000 μm²) of extrasynaptic α-Bgtx-stained (AChR) spots in fibres of old muscles. (P1–P3) Representative images of the Sol muscle double immunolabelled for VAcHT (green) and NF (blue) and stained with α-Bgtx (red); arrows point to (P3) α-Bgtx-stained AChR spots that exhibit both (P1) VAcHT and (P2) NF positivity; the merged image for the three channels is shown in (P4). Scale bars: In (J2) = 20 μm [valid for (F1–J1)]; in (N) = 20 μm [valid for (K–M)]; and in (P4) = 30 μm [valid for (P1–P3)]. EDL, extensor digitorum longus; Gra, gracilis.

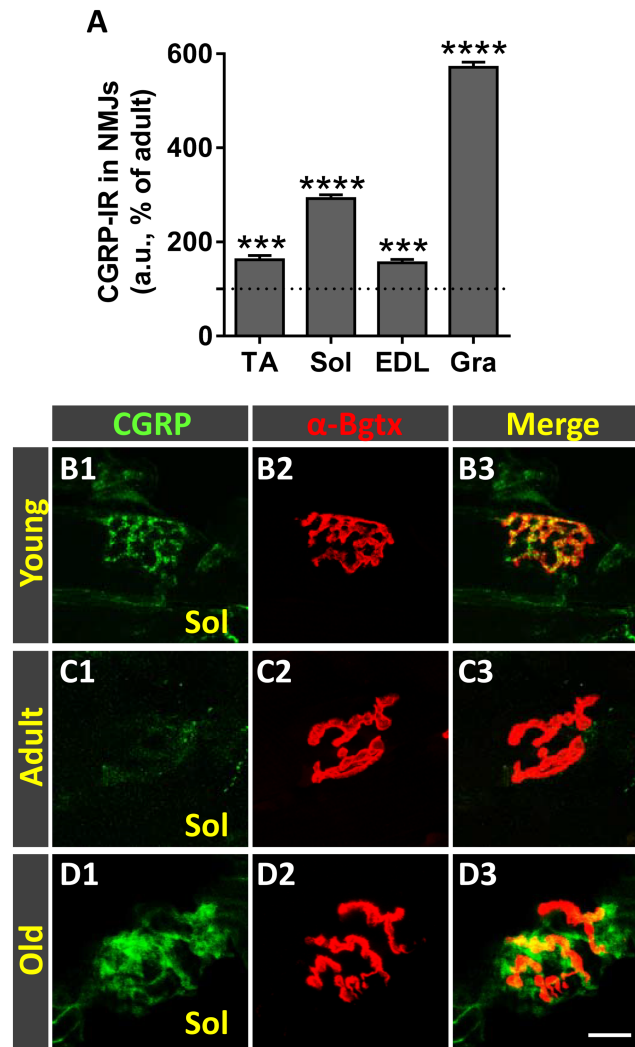


Figure 8 Ageing is accompanied by an increased expression of calcitonin gene-related peptide (CGRP) in neuromuscular junctions (NMJs) of hindlimb muscles. (A) Changes in CGRP immunoreactivity (IR) in NMJs of old tibialis anterior (TA), soleus (Sol), extensor digitorum longus (EDL), and gracilis (Gra) muscles expressed as the percentage of increase compared with respective adult muscles. (B1–D3) Representative confocal micrographs of CGRP-immunostained (green) NMJs of Sol muscles from young, adult, and old mice; sections were also stained with α -bungarotoxin (α -Bgtx) (red) for endplate identification. Data in the graphs are expressed as the mean \pm SEM, *** P < 0.001 and **** P < 0.0001 vs. adult (one-way ANOVA and *post hoc* Bonferroni's test); one muscle for each muscle type taken from four adult and five old mice was used for analysis; 80–100 NMJs per muscle type were examined. Scale bar in (D3) = 10 μ m [valid for (B1–D2)].

were seen in old animals compared with adults (muscle weight reduction: \sim 23% Sol and \sim 43% EDL) (Figure 11A). No significant differences were obtained when muscle weights were normalized to body weight (muscle mass/body weight) (Figure 11B). Gra muscles from old mice exhibited even higher (although not significant) normalized weights compared with those from adults. Additionally, compared with adult muscles, old muscles did not exhibit significant changes in cross-sectional areas (Figure 11C). We next analysed the density of myofibers and found a reduction in the Sol and EDL muscles of old animals, with the most prominent decrease observed in the EDL muscle (myofiber density reduction: \sim 24% Sol and \sim 37% EDL). This indicates that a

differential decline in the proportion of myofibers occurs in distinct type of muscles with ageing. The effect of ageing on myofiber size was analysed in muscle cross sections immunolabelled for laminin and showed no significant differences in the average myofiber size between adult and old animals for all the muscles examined (Figure 11E). Nevertheless, compared with adult muscles, increased contents of connective tissue were found in all muscles from old animals, this increase being more marked in the EDL (Figure 11F).

In agreement with previous reports,⁶⁷ all the old hindlimb muscles analysed exhibited high proportions of myofibers showing centrally located nuclei (Figure 11G–O). In young muscles, only a small percentage (0.5–1.5%, depending on

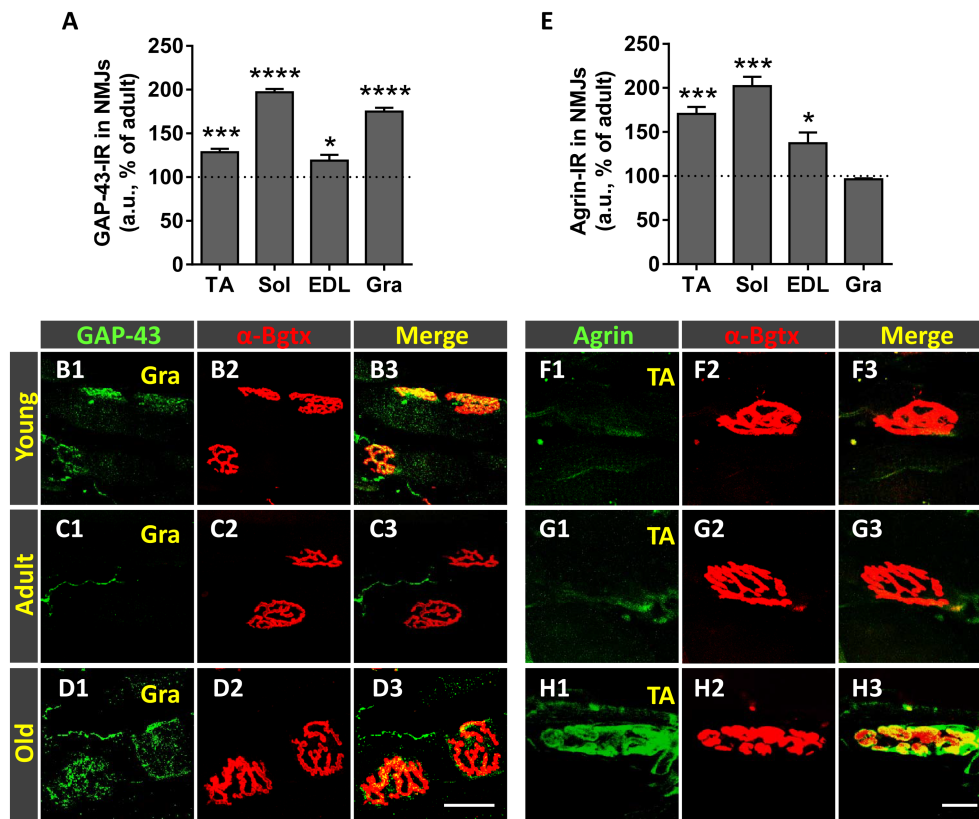


Figure 9 Age-related changes in growth associated protein 43 (GAP-43) and agrin expression in in neuromuscular junctions (NMJs) of hindlimb muscles. Changes in (A) GAP-43-immunoreactivity (IR) and (E) agrin-IR (in arbitrary units [a.u.]) in NMJs of old tibialis anterior (TA), soleus (Sol), extensor digitorum longus (EDL), and gracilis (Gra) muscles expressed as the percentage of increase compared with adult respective muscles. Representative confocal images of NMJs of TA and Gra muscles from young, adult, and old mice immunostained for (B1–D3) GAP-43 and (F1–H3) agrin, both in green; muscle sections were also stained with α -bungarotoxin (α -Bgtx) (red) for endplate identification. Data in the graphs are expressed as the mean \pm SEM, * $P < 0.05$; *** $P < 0.001$, and **** $P < 0.0001$ vs. adult muscles (one-way ANOVA and *post hoc* Bonferroni’s test); one muscle for each muscle type taken from four adult and five old mice was used for analysis; 80–100 NMJs per muscle type were examined. Scale bars: In (D3) = 10 μ m [valid for (B1–D2)] and in (H3) = 10 μ m [valid for (F1–H2)].

the muscle) of myofibers displayed central nuclei. These numbers significantly increased in old muscles, this increase being more prominent in the TA and Gra muscles (~12% and 18%, respectively) (Figure 11G). Because the presence of central nuclei in a myofiber can be considered as an indicator of its regeneration following degeneration,^{87,88} these results suggest that over the ageing process, all limb muscles examined undergo, to some extent, fibre degeneration and attempt to regenerate these lost fibres.

Satellite cells (SCs) are muscle-resident stem cells required for sustained muscle regeneration.^{89,90} SCs express paired box protein 7 (Pax7), a transcription factor involved in the proliferation of muscle precursor cells. To analyse age-related changes in SCs, immunocytochemistry for Pax7 was combined with DAPI staining in sections of adult and old mouse muscles. Compared with adult muscles, decreased numbers of Pax7-positive SCs were observed in all examined muscles from old animals, although SC depletion only attained statistical significance in Sol and EDL muscles (Figure 11P–S3).

From studies mainly performed in rats, it has been documented that ageing is associated with changes in the fibre type profile of skeletal muscles. Thus, a transition from fast (type 2) to slow (type 1) fibres, leading to a preponderance of the latter, appears to occur in aged muscles.^{91,92} We analysed the fibre type (1, 2A, and 2B) composition of selected muscles by using different isoform-specific anti-myosin heavy chain (I, IIA, and IIB) antibodies. As previously reported,^{68,93} in adult mice, the Sol muscle was seen to be mainly composed of slower fibres (types 1 and 2A), whereas EDL and TA muscles showed a predominance of fast fibres (type 2B > 2A in EDL and type 2A > 2B in TA); the Gra, which is the more proximal hindlimb muscle, also consisted predominantly of types 2A and 2B fibres (2A > 2B), with a lower proportion of type 1 fibres. These myofiber type profiles exhibited differential changes with ageing. Compared with adult muscles, all old distal hindlimb muscles analysed (TA, EDL, and Sol) displayed a significant reduction in the proportion of type 2B fibres, whereas the amount of type 2A fibres was found significantly

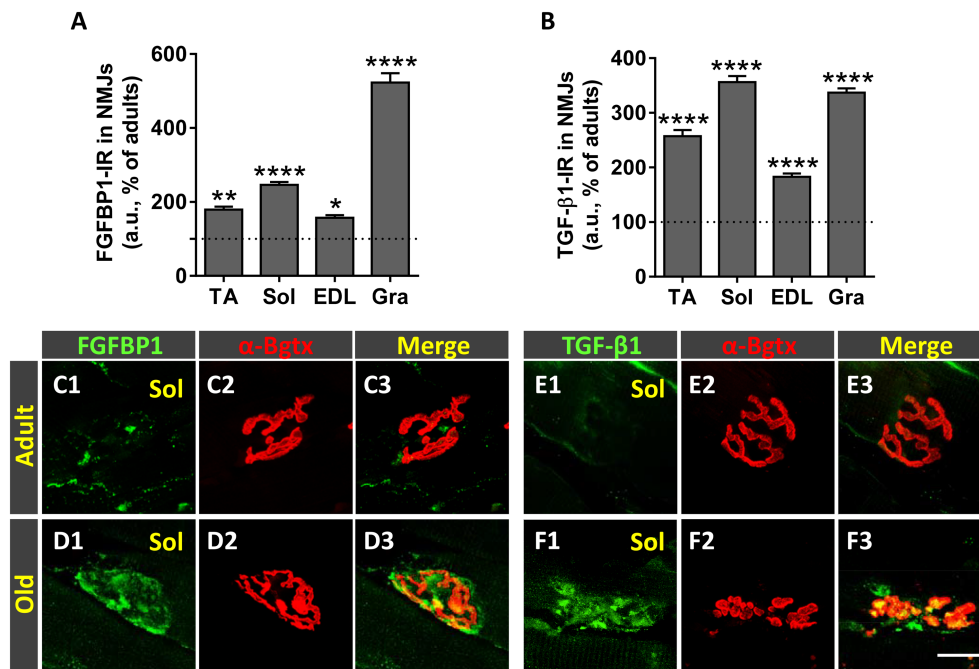


Figure 10 Age-related changes in fibroblast growth factor binding protein 1 (FGFBP1) and transforming growth factor-β1 (TGF-β1) expression in neuromuscular junctions (NMJs) of hindlimb muscles. Quantification of changes in (A) FGFBP1-immunoreactivity (IR) and (B) TGF-β1-IR (in arbitrary units [a.u.]) in NMJs of tibialis anterior (TA), soleus (Sol), extensor digitorum longus (EDL), and gracilis (Gra) muscles of old mice; changes are expressed as the percentage of immunostaining increase compared with adult NMJs. Representative confocal micrographs of NMJs of Sol muscles from adult and old mice immunostained for (C1–D3) FGFBP1 and (E1–F3) TGF-β1, both in green, as indicated; muscle sections were also stained with α-bungarotoxin (α-Bgtx) (red) for endplate identification. Data in the graphs are expressed as the mean ± SEM, * $P < 0.05$, ** $P < 0.01$, and **** $P < 0.0001$ vs. adult muscles (one-way ANOVA and *post hoc* Bonferroni's test); one muscle for each muscle type taken from four adult and five old mice was used for analysis; 80–100 NMJs per muscle type were examined. Scale bar in (F3) = 20 μm [valid for (C1–F2)].

decreased in the TA and EDL but dramatically increased in the Sol. Additionally, all these old muscles showed a reduced proportion of type 1 myofibers with respect to adult muscles, but only in the case of the EDL, this decline attained significance (Figure 12A–M). Conversely, compared with adult mice, the Gra muscle of old animals exhibited a prominent increase in the proportion of types 1 and 2B fibres and a reduction in the content of type 2A fibres (Figure 12A–M). These findings contrast with those obtained in previous studies performed in rat skeletal muscles, in which it has been reported that ageing results in a switch from type 2A to type 1 fibres in the slow Sol muscle and from type 2B to type 2X (a type of fibre having a resistance to fatigue intermediate between type 2A and type 2B fibres) in fast muscles.^{94,95}

Lipofuscin, often called 'age pigment', consists of polymorphous and non-degradable autophagocytosed material that, coming from different intracellular structures, accumulates in lysosomes. The presence of lipofuscin in a cell is considered the result from an oxidative stress process, in which oxidized compounds, mainly of lipid and protein origin, are resistant to hydrolysis by lysosomal enzymes.^{96,97} Lipofuscin has a broad autofluorescence and, when excited by lights of diverse wavelengths in combination with proper barrier filters, is easy to distinguish from immunolabelled fluorescent

structures.⁹⁸ In our study, in comparison with muscles from adult animals in which no lipofuscin aggregates were seen, all the examined muscles from old mice exhibited prominent lipofuscin accumulation (Figure 12N). This was especially prominent in the Gra muscle, compared with the slow-twitch Sol muscle showing the smallest amount of lipofuscin aggregates. Within the muscle, the proportion of lipofuscin granules varied considerably between myofibers, and some of them appeared completely devoid of this pigment (Figure 12O and P). Interestingly, in all muscles, the largest fibres were those which exhibited the highest levels of lipofuscin accumulation (Figure 12Q). The correlation between fibre type and accumulation of lipofuscin was explored in the old TA muscle. We observed that type 1 fibres exhibited a significantly lower content of the pigment compared with types 2A and 2B fibres (Figure 12R).

Discussion

Despite the notable progresses made in the knowledge of the etiological factors leading to ageing sarcopenia, the precise causative mechanisms are far from fully understood. The intricate interactions between the distinct types of cells and

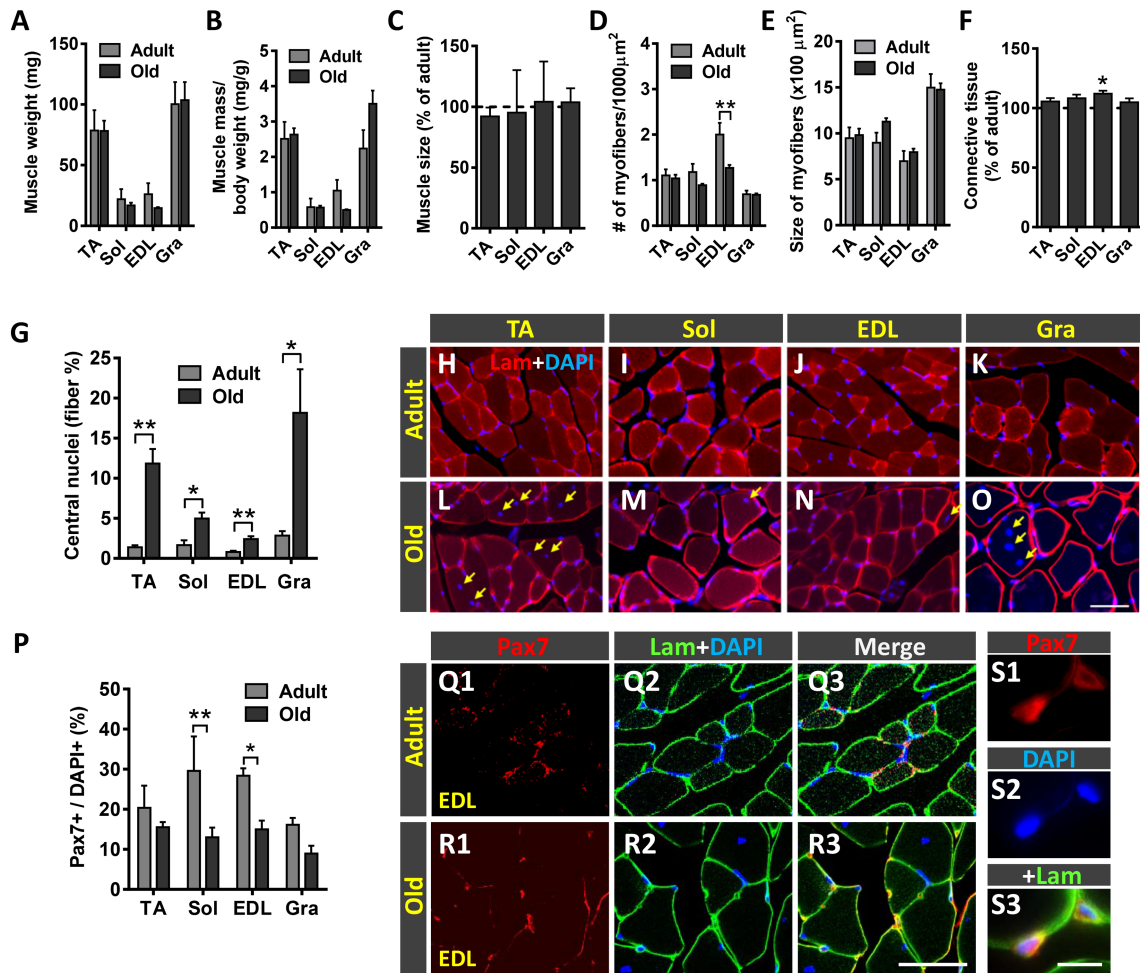


Figure 11 Effect of ageing on the histology of tibialis anterior (TA), soleus (Sol), extensor digitorum longus (EDL), and gracilis (Gra) muscles. (A) Wet weight of muscles (in mg) and (B) weight of muscles relative to body weight (expressed in mg/g). (C) Changes in the total cross-sectional area of old muscles (expressed as the percentage with respect to adult muscles). (D) Density of fibres in muscles (expressed as the number of myofibers in 1000 µm² muscle cross-sectional area). (E) Average myofiber size (cross-sectional area in µm²) of the muscles. (F) Changes in the content of connective tissue in old muscles (expressed as the percentage with respect to adult muscles). (G) Proportion of myofibers exhibiting central nuclei. (H–O) Representative images of transversal muscle sections, double labelled with an antibody against laminin (lam) and 4',6-diamidino-2-phenylindole dihydrochloride (DAPI) for DNA. (P) Percentage of paired box protein 7 (Pax7)-immunostained cells (satellite cells) with respect to DAPI-positive nuclei in adult and old muscles. Representative confocal images of Pax7 immunostaining (red) combined with immunolabelling for laminin (green) and DAPI staining (blue) in (Q1–Q3) adult and (R1–R3 and S1–S3) old EDL muscle sections. A higher magnification view of Pax7 immunostaining in old EDL muscle is shown in (S1–S3). Data in the graphs are expressed as the mean ± SEM, **P* < 0.05, ***P* < 0.01, and ****P* < 0.001 vs. adult; *n* = 5–6 muscles for muscle type from different animals and age; number of fibres examined per muscle and mouse: (D and E) = 200, (G) = 3,000, and (P) = 100. Scale bar in (O) = 50 µm [valid for (H–N)]; (R3) = 40 µm [valid for (Q1–R2)]; and (S3) = 10 µm [valid for (R1–R2)].

tissues shaping the neuromuscular system are complex and hard to interpret in isolation. Indeed, results reported in the literature are sometimes ambiguous, with strong divergences in results obtained from different ageing models.⁹⁹ Rodents, mainly various rat and mouse strains, have been widely used in studies of sarcopenia. Although it is unlikely that the ageing processes in these animal models are entirely comparable with those in humans, rodents provide an experimental paradigm that allow us to overcome the obvious problems inherent to human long lifespan, environmental and nutrition conditions, and tissue sampling.⁹⁹ However, most of the ageing research

performed in murine models has been restricted to specific constituents of the neuromuscular system, providing a partial view of cellular and molecular alterations leading to sarcopenia. In an attempt to unify and clarify discrepant published data, we conducted a detailed analysis of ageing-related structural and functional alterations in the neuromuscular system of the C57BL/6JRj mouse, a well-established model for sarcopenia. Here, all the main cellular components were simultaneously examined in each individual animal at specific time points. Additionally, changes in some key molecules with well-established roles in the development

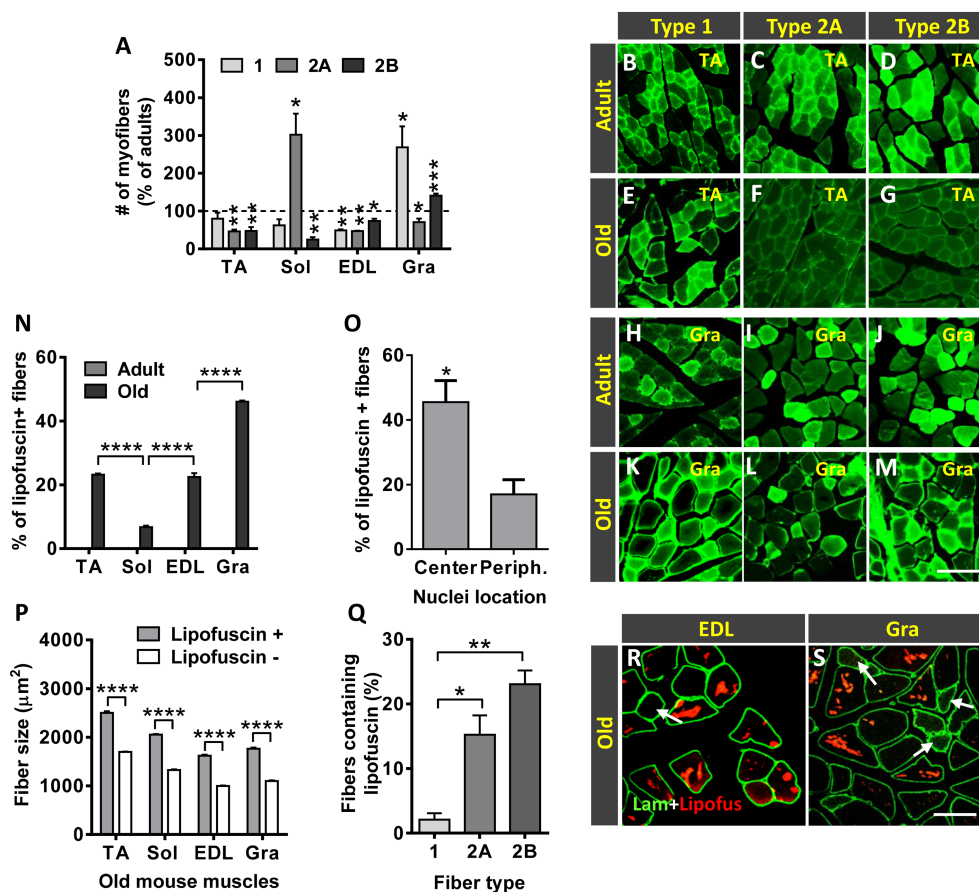


Figure 12 Age-related changes in fibre type composition and lipofuscin accumulation. (A) Changes in myofiber type composition in the old tibialis anterior (TA), soleus (Sol), extensor digitorum longus (EDL), and gracilis (Gra) muscles expressed as the proportion of types 1, 2A, and 2B fibres compared with respective adult muscles ($^*P < 0.05$ and $^{**}P < 0.01$ vs. respective adult muscles; Student's *t*-test). Representative images of (B–G) TA and (H–M) Gra muscles from (B–D and H–J) adult and (E–G and K–M) old mice, showing myosin heavy chain I, IIA, and IIB immunostaining to demonstrate types 1, 2A, and 2B myofibers, as indicated. (N) Percentage of fibres containing lipofuscin granules in muscles from adult and old mice. (O) Percentage of old TA muscle fibres with central or peripherally located nuclei containing lipofuscin aggregates. (P) Average size (cross-sectional area in μm^2) of myofibers with or without lipofuscin granules. (Q) Percentage of types 1, 2A, and 2B myofibers containing lipofuscin in the TA muscle of old mice. (R and S) Representative fluorescent images of EDL and Gra muscle sections processed for laminin immunostaining (green); lipofuscin autofluorescence was excited using 510–560 nm excitation and 590 nm emission filters; note that fibres with a small size are devoid of lipofuscin aggregates (arrows). Data in graphs are shown as the mean \pm SEM of fibres analysed from four adult and five old muscles of different animals (number of examined myofibers per muscle: (N and O) = 400–700; (P and Q) = 300–500 ($^*P < 0.05$, $^{**}P < 0.01$, $^{***}P < 0.001$, and $^{****}P < 0.0001$; one-way or two-way ANOVA and *post hoc* Bonferroni's test). Scale bars: (M) = 50 μm [valid for (B–L)] and (S) = 100 μm [valid for (R)].

and maintenance of neuromuscular innervation were also examined. A summary of the main results of this study is depicted in *Figure 13*.

We reported that ageing is not accompanied by significant MN death in the lumbar spinal cord of mice. Although the presence of a certain degree of MN degeneration cannot be excluded, our results suggest that MN loss should be considered as a minor event in the context of the neuromuscular changes occurring during ageing. This finding is in contrast with results from previous works in rodents^{9,15–17} and humans,^{14,41} in which significant MN death has been reported with ageing. Our results, however, are consistent with data from studies that have shown the absence of MN

degeneration at advanced ages.^{21,22,100} The disparity in all these results could be ascribed to differences in the animal model species and age of animals included in the studies, segments of the spinal cord analysed, and the procedures utilized for MN counting. Thus, most of the mentioned studies have been performed in different rat strains and, in some cases, without gender segregation. In the present analysis, we only used male mice classified into three age groups, with a strict age delimitation. Moreover, we counted the total number of MNs in serial sections of the entire lumbar spinal cord by using a standard and reliable procedure widely applied in the literature (see Clark and Oppenheim³⁷ and also Calderó *et al.*^{38,101}), which allows an accurate estimation of

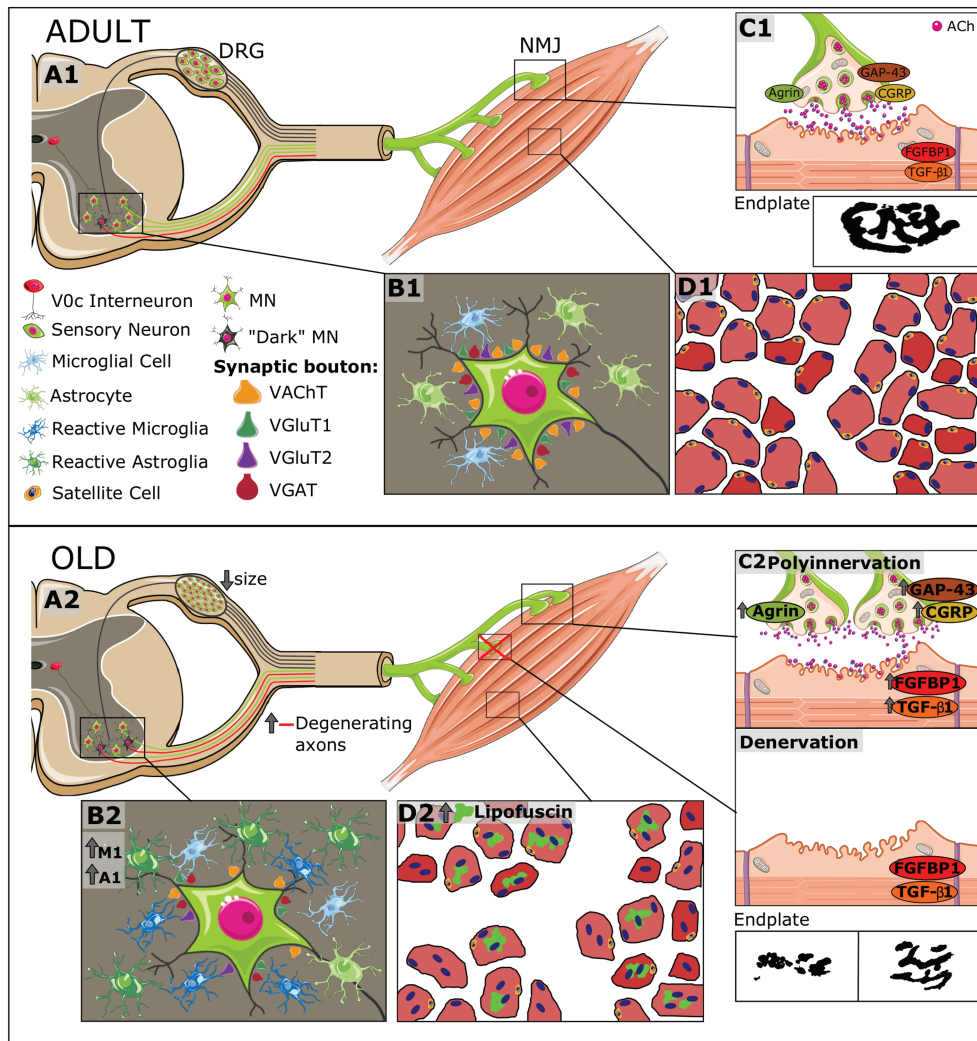


Figure 13 Overview of age-associated changes in the mouse neuromuscular system. (A1–D1) The structural organization of the different components of the system, including spinal cord motoneurons (MNs), neuromuscular junctions (NMJs), skeletal muscles, and dorsal root ganglion (DRG) sensory neurons, is schematically represented. MNs, located in the ventral horn, project their axons throughout the ventral roots; motor nerve terminals establish synaptic contacts with skeletal muscle fibres (NMJs). (B1) In normal conditions, adult spinal MNs receive abundant synaptic inputs (synaptic boutons), which can be identified by means of vesicular acetylcholine transporter (VACHT) (excitatory cholinergic), vesicular glutamate transporter 1 (VGlut1) and vesicular glutamate transporter 2 (VGlut2) (excitatory glutamatergic), and vesicular GABA transporter VGAT (inhibitory GABAergic) markers. (A1) Glutamatergic (VGlut1-positive) afferents to MNs come from proprioceptive (parvalbumin-positive) sensory neurons located in the DRG; cholinergic afferents (C-boutons) to MNs come from a small cluster of cholinergic interneurons (V0c), which are located near the central canal of spinal cord. (B1) Spinal MNs are surrounded by abundant microglial and astroglial cells, which are in a resting state. The vast majority of MNs show a ‘healthy’, lightly haematoxylin and eosin-stained appearance; intermixed with them, some abnormally dark MNs can be occasionally seen in adult spinal cords; these dark MNs could account for the presence of some degenerating motor axons that can be already observed in ventral roots of adult mice. In adult muscles, both presynaptic and postsynaptic elements of NMJs exhibit a well-organized and ‘healthy’ appearance: smooth nerve terminals enter in endplates displaying a ‘pretzel-like’ pattern; (C1) adult NMJs exhibited low levels of agrin, growth associated protein 43 (GAP-43), calcitonin gene-related peptide (CGRP), fibroblast growth factor binding protein 1 (FGFBP1), and transforming growth factor-β1 (TGFβ1). (D1) Diagram of adult myofibers surrounded by connective tissue as can be seen in a transverse muscle section. (A2–D2) In the course of ageing, there is (i) an increase in the number of dark MNs; (ii) a reactive gliosis in ventral horn with a raise in the proportion of harmful M1 microglia and A1 astroglia; (iii) a marked loss of excitatory (cholinergic and glutamatergic) synaptic afferents and reduction in the size of GABAergic synaptic boutons on MNs; (iv) an increase in the proportion of degenerated motor axons and the existence of signs of nerve sprouting and regeneration; and (A2 and B2) (v) an atrophy of sensory proprioceptive and nociceptive DRG neurons and increased expression of their markers. (C2) Muscles of old mice exhibit signs of either polyinnervation or denervation and fragmentation of endplates; these changes are accompanied by the increased expression of agrin, GAP-43, CGRP, FGFBP1, and TGF-β1, suggesting an active process of NMJ remodelling and muscle reinnervation. Moreover, old muscles show numerous fibres with lipofuscin accumulation and centrally positioned nuclei, indicative of muscle regeneration, and fibrotic tissue deposition between fibres; (D2) the proportion of satellite cells were also markedly reduced in old muscles.

neurons that die. This systematic approach is not often employed in other studies. Although we did not find a significant reduction in the total number of MNs in old mice compared with that in adult animals, we noticed a modest decrease in the number of MNs located in the anterolateral column, without changes in the anteromedial and intermediate columns. Because MNs from the anterolateral column innervate distal hindlimb muscles, this finding is consistent with the more prominent age-related involutive changes occurring in these muscles.

Additionally, it is important to note the presence of MNs with an altered histological appearance (dark MNs) scattered across the lumbar spinal cord, particularly in the intermediate column. Dark neurons have been described in healthy and pathological brains of different animal models,¹⁰² but it remains unclear whether they are the result from a pathological change or merely represent an artefact. In this regard, an inappropriate tissue specimen fixation, particularly the time intervals between collecting samples and fixation, appears to provoke an increase in the proportion of dark cells in the nervous tissue.¹⁰³ Although we cannot completely exclude that dark MNs are a consequence of tissue fixation defect, this possibility appears unlikely because all our animals were intracardially perfused and the spinal cords were rapidly removed and subsequently postfixed. The fact that dark MNs might reflect damaged cells is supported by the presence of this type of neurons in the brain cortex and hippocampus following traumatic brain injury or focal cerebral ischemia.^{104,105} Nevertheless, the fate of dark neurons is not still clear. Although it has been generally assumed that dark neurons are 'sick' cells prone to die and would be subsequently eliminated, it is presently proposed that a number of them undergo reactive mechanisms for cell death prevention. Whether or not surviving neurons can conduct their appropriate functions remains to be elucidated.^{102,104} In our analysis, the proportion of dark MNs, although increased with age, did not significantly change in old animals compared with adult mice. Even considering that a certain number of dark MNs undergo degeneration, only a minor proportion of them would finally die. Indeed, we found that the number of 'healthy', lighter stained, MNs did not exhibit a significant decline in the course of ageing. On the other hand, we noticed no significant reduction in the proportion of MMP-9 MNs in spinal cord of old animals, suggesting that vulnerable fast MNs do not necessarily die during the ageing process.

The presence of dark, presumably sick, MNs in the spinal cord of adult mice fits well with the pattern of changes we observed in VRs. Previous work performed in young (2–4 months) and old (22–25 months) mice has shown that in the latter, VR motor axons displayed alterations in diameter ratios and myelin, indicative of age-associated axonal degeneration⁸²; in this study, however, no significant decline in the number of motor axons has been found with ageing. Here, we noticed that although in a low proportion, some motor

axons located in VRs of adult animals displayed signs of degeneration and myelin inclusions. These alterations markedly increased in VRs of middle-aged mice, in which numerous myelin spheroidal inclusions and Wallerian-like degenerative changes are often seen. Interestingly, middle-aged (14 months) VRs exhibited increased numbers of clusters of small myelinated axons, which likely are new nerve sprouts originated from healthy axons. Overall these findings suggest that sustained cycles of degeneration/regeneration and sprouting from healthy axons occur, to greater or lesser degrees, throughout the lifespan. We assume that these degeneration/regeneration cycles are exacerbated in older mice, in an attempt to compensate for the loss of motor terminal branches and synaptic sites in muscle.

Although MN death does not appear to be a relevant pathological process over the course of ageing, we cannot rule out the possibility that MNs with a normal histological appearance may have impaired function. In fact, we provide here strong evidence that MNs of old animals suffer a prominent loss of excitatory cholinergic and glutamatergic inputs, which is in agreement with recent reports.^{100,106} Although we noticed no age-associated changes in the density of inhibitory GABAergic synapses, their size on old MNs was found significantly reduced. MN deafferentation has also been widely reported by us and others in murine models of MN diseases, such as spinal muscular atrophy (SMA)^{107–111} and amyotrophic lateral sclerosis (ALS),^{109,112–115} and also following nerve injury.^{116,117} Data from studies performed in these paradigms support the idea that the loss of synaptic inputs is a process that precedes MN degeneration and that a significant degree of deafferentation is not necessarily associated to MN death.¹⁰⁷ This assumption is in agreement with the absence of MN loss we found in the present work. It is reasonable to assume that alterations in central synapses may negatively impact on MN integrity and function. It is well known that MN excitability is finely regulated by afferent synaptic inputs, which mediate the generation of co-ordinated firing patterns leading to muscle contractions.¹¹⁸ Because the accurate control of MN excitability is critical for a proper motor behaviour, it is obvious that the latter can be markedly impaired by MN deafferentation. Thus, overall, our results indicate that MN dysfunction, rather than cell death, could explain the changes in motor skills and in electromyography recordings seen in our study.

An interesting finding in the present study is the prominent microgliosis and astrogliosis found around aged MNs. This result indicates that ageing is accompanied by a neuroinflammatory response in spinal cord ventral horn, as it has been documented in different brain regions in healthy elderly (reviewed in previous studies^{119–121}). Ageing-related chronic reactive gliosis has been associated to an increased vulnerability of aged brain to neurodegenerative diseases. Indeed, neuroinflammation has been reported to occur in a number of neurodegenerative processes, including the MN

disorders ALS and SMA.^{56,107,108,110,122–124} The role of neuroinflammation in chronic neurodegeneration, and particularly in MN diseases, has still to be clarified. It is now accepted that glial reaction in these pathologies may have either detrimental (cytotoxic) or beneficial (neuroprotective) effects on MNs.¹²⁴ In this regard, depending on the type of stressor triggering the gliosis process, both microglia and astroglia can achieve M1 and A1 (pro-inflammatory) or M2 and A2 (anti-inflammatory) reactive functional phenotypes, respectively.^{53,58} Moreover, M1 and A1 reactive cells can turn into M2 and A2 phenotypes, respectively, and vice versa, according to the environment in which they are activated. In fact, M1–A1 and M2–A2 phenotypes represent the extremes of a continuum range of distinct reactive states. The dynamic and bidirectional transformation of M1/M2 and A1/A2 phenotypes seems to play a critical role in neurodegeneration, in which neuronal damage has been related to a sustained activation of M1 and A1 cells resulting in an imbalance between the two microglial (M1/M2) and astroglial (A1/A2) subpopulations. Additionally, activated M1 microglia can induce neurotoxic A1 astrocytes, which have been found to be abundant in diverse human neurodegenerative diseases,⁶¹ indicating a cross-talk between microglia and astrocytes in neuroinflammation. We show here that gliosis in the aged spinal cord is accompanied by a prominent increase in harmful M1 microglia and A1 astroglia, with a reduction in the proportion of neuroprotective M2 and A2 phenotypes. A recent study has reported that the depletion of microglia is able to prevent or reverse the loss of muscle innervation in aged mice¹²⁵; this finding suggests an important pathogenic role of neurotoxic microglia in the age-related neuromuscular decline, although the mechanism by which microglia exert their detrimental actions in ageing is not known. It has been shown that both microglia and astrocytes are involved in synapse elimination during neurodegeneration.¹²⁶ A similar function has been ascribed to astrocytes in actively eliminating defective synapses.¹²⁷ The correlation between gliosis and MN deafferentation, found here in the old spinal cord, suggests a possible function of glial cells in the synapse elimination during ageing, as it has also been reported for ALS and peripheral nerve injury.^{57,126} However, to our knowledge, no published data exist on whether neuroinflammatory glial cells actually eliminate synapses on diseased MNs. In a recent study using a model of sciatic nerve axotomy, we found no evidence of synaptic bouton enwrapping and phagocytosis by microglia but noticed that microglial processes, recruited by lesioned MNs, are in close contact with degenerating afferent synaptic terminals, suggesting an active role of microglia in the disintegration of adjacent presynaptic terminals on MNs.⁵⁷ It has been reported that activated microglia can produce molecules (i.e. nitric oxide, oxygen radicals, proteases, and cytokines), which can induce neuronal damage and/or the extracellular digestion of synaptic debris.¹²⁸ A question that needs to be answered is whether glial activation in aged

spinal cord is a primary event leading to the loss of normal functional synaptic inputs to MNs with a subsequent neuronal damage or, conversely, is a secondary response to an altered synaptic function,¹²⁹ as appears to occur in damaged MNs after peripheral nerve transection.⁵⁷

In this context, we found that ageing-related spinal cord central synapse loss is accompanied by changes in DRG sensory neurons. We noticed that with ageing, nociceptive (CGRP-positive and IB4-positive) and proprioceptive (PV-positive) DRG neurons exhibited significant changes in their numbers and expression levels of their markers and atrophy of cell soma. Sensory neurons showed increased expression of CGRP and PV and higher staining with IB4. The increased proportion of DRG PV-positive neurons differs from previous data by Vaughan *et al.*¹³⁰ showing no significant changes in the numbers of DRG PV-positive neurons between middle-aged (11- to 13-month-old) and old (15- to 21-month-old) mice. Differences between both studies could be related to mouse strains used because genetically modified mice were utilized in Vaughan's work. In our study, however, neuron atrophy in old DRGs was particularly evident in proprioceptive large, PV-positive neurons, which are the source of the major synaptic inputs (Ia VGlut1 afferents) to MNs. Ia afferents establish selective excitatory monosynaptic connections with spinal MNs that, in turn, project their axons to the same or related (homonymous or synergistic, respectively) muscles from which they receive sensory feedback.¹³¹ This circuitry, which is essential for motor coordination and posture, appeared to be impaired in old animals, as inferred from progressive age-related alterations in mobility observed in open field analysis. On the other hand, changes in the proportion of DRG neurons expressing CGRP and in the levels of this neuropeptide have been reported to occur in various inflammatory pain models.^{132–135} Therefore, the increased numbers of DRG neurons expressing CGRP found in our study are in concordance with the state of general, low-grade, chronic inflammation that appears to be linked to elderly, which has been considered an etiological factor of ageing sarcopenia. In this regard, a systemic increase in pro-inflammatory mediators coming from different sources has been reported to occur in advanced ages.²

Nerve conduction studies allow the functional quantitative assessment of large myelinated fibres. Thus, the amplitude of the evoked action potentials is an index of the number of conducting nerve fibres and the peripheral innervation, whereas the nerve conduction velocity is related to axonal calibre and myelination.¹³⁶ The nerve conduction tests performed indicate that the conduction of impulses is reduced in advanced age, which is in agreement with previous reports in laboratory animals^{137–139} and in humans.^{140–142} In this regard, a previous longitudinal evaluation in mice has shown that motor and sensory nerve conduction velocity increased during young adult life, and then remained unchanged until the last third of the lifespan, when it tended to decline.¹³⁹

Additionally, age-associated reduction in the amplitude of motor and sensory nerve action potentials has also been reported in animals^{138,139} and humans.^{140,141,143} Our present results also indicate that the amplitude of CMAPs and CNAPs tend to decrease with ageing, particularly in distal targets, such as foot muscles and toe nerves. In fact, a slow loss of myelinated fibres in peripheral nerves with ageing has been demonstrated in several animal species.^{140,144–146} Indeed, in a detailed morphometrical study in mice, we have found that after 20 months of age, the sciatic nerve showed a noticeable loss of both unmyelinated and myelinated axons, accompanied by a decrease in axonal size and myelin thickness.¹⁴⁶ The effect of sustained pressure on the paws over life has been attributed as one of the determining factors for the particular functional loss of plantar muscles compared with more proximal and tail muscles,¹⁴⁵ as we have observed here in old mice.

MUNE analysis reflects well the potential loss of MNs with ageing.¹⁴⁷ The reduction in MUNE found here in old mouse muscles was only mild and is in agreement with the absence of significant MN degeneration. Following loss of an MN, motor axons are able to sprout collateral branches within the own muscle and thus increase the size of the corresponding motor unit,¹⁴⁸ allowing an efficient compensatory mechanism for maintaining muscle force. However, with advanced ageing, the capability for collateral sprouting¹⁴⁹ and maintenance of size after expansion of the motor unit¹⁵⁰ is defective. In addition, alterations of NMJ function as a consequence of alterations in fast-twitch, fast-fatigable motor units have been described in aged rodents,¹⁵¹ which cause a decrease in the mean size of remaining motor units, as we found here.

Whether NMJs are stable over the lifespan and if they change their morphology with ageing are debatable. Some early studies in rabbits and cats have shown that a certain degree of nerve sprouting and a continuous turnover of NMJs occur in normal muscles.¹⁵² However, more recent data in mice and humans support the idea that NMJs are generally stable for most of the lifespan.^{28,153} In agreement with previous published reports,^{67–69,82,154} we found, in old muscles, a significant amount of NMJs exhibiting conspicuous plastic changes, including partial or complete denervation, polyinnervation, increased nerve terminal branching complexity, and sprouting. Moreover, overt signs of endplate fragmentation and ectopically innervated AChR clusters throughout the myofiber were seen in old muscles. Overall, these observations fit with the hypothesis that ageing entails a continuous process of muscle denervation/reinnervation (reviewed in Larsson *et al.*⁶). In this regard, we noticed that aged muscles displayed a significant increase in some molecules having specific roles in development, maturation, plasticity, and stability of NMJs. These molecules include CGRP, GAP-43, agrin, FGFBP1, and TGF- β 1. CGRP, GAP-43, and agrin are developmentally regulated proteins, which are synthesized in MN cell bodies and axonally transported to

nerve terminals, where they are released and exert their function. Whereas GAP-43 is highly expressed in the growth cones of motor axons and are involved in developmental axonal outgrowth,⁷¹ agrin plays a crucial role in the initiation of NMJ formation by clustering AChRs and, also, in the preservation and regeneration of the adult NMJ.^{74,75} On the other hand, in the neuromuscular system, CGRP has been proposed to act as a communication molecule between MNs and skeletal muscles and is involved in the development and maintenance of NMJs and muscle cells^{155,156}; motoneuronal CGRP is up-regulated following nerve injury, but its raised levels decline with the morphological and functional recovery of motor innervation, suggesting a function of the neuropeptide in axonal growth and NMJ plasticity.^{49,50,157,158} On the whole, these three molecules were found in low levels in muscles of adult mice compared with young animals but were clearly up-regulated in motor nerve terminals of old muscles. This finding suggests an active role for these proteins in the regulation of the compensatory nerve terminal sprouting and reinnervation of denervated muscles in ageing.

The FGFBP1 has been found to be up-regulated in skeletal muscles of a mouse model for SMA.¹⁵⁹ More recently, it has been described that NMJs of normal adult muscles express and concentrate FGFBP1, but its levels decrease when NMJs undergo pathophysiological changes as occurred in the SOD1^{G93A} mouse model for ALS.⁷⁹ Compared with the relative high intensity of immunostaining for FGFBP1 observed in NMJs of young muscles (not shown), we found that FGFBP1-immunolabelling markedly declined in adult NMJs but increased again in old NMJs, particularly in those of the Gra muscle. The increased content of FGFBP1 in old muscles is in concordance with its proposed function in promoting NMJ repair⁷⁸ and suggests a role of this protein in the process of age-related NMJ remodelling and muscle reinnervation. The elevated levels of FGFBP1 noticed by immunocytochemistry in old muscles contrast with the findings by Valdez's group,⁷⁹ which have reported a significant reduction in FGFBP1 transcripts in the TA muscle of 24-month-old mice. This divergence could be explained by the differences in methodology and animals used in this latter study,⁷⁹ in which the FGFBP1 expression levels have been examined by quantitative PCR in aged wild-type heterozygous (FCFBP1^{+/-}) animals of homozygous (FCFBP1^{-/-}) FGFBP1 knockouts. Nevertheless, in agreement with data from this same study, we found higher contents of TGF- β 1 in muscles of young and old animals than in those of adult mice. Our findings showing increased levels of both TGF- β 1 and FGFBP1 in old muscles *in vivo* are difficult to reconcile with the suggested role of TGF- β 1 in inhibiting FGFBP1 expression found in cultured myotubes.⁷⁹ However, the increased levels of TGF- β 1 could explain some changes found in muscles of old mice. Alterations in the expression of TGF- β 1 and its signalling pathways have been associated with inherited and acquired myopathies (reviewed in Burks and Cohn¹⁶⁰). In this regard,

an increase in circulating TGF- β 1 levels has been found to be associated with sarcopenia. TGF- β 1 is considered a potent regulator of tissue wound healing and fibrosis in the skeletal muscle¹⁶¹ and appears to play an important role in promoting the transformation of myoblasts in myofibroblastic cells. Myofibroblasts have been involved in tissue fibrosis and could be responsible for the increased proportions of connective tissue we found in old muscles. It has been proposed that elevated systemic or local levels of TGF- β 1 and skeletal muscle fibrosis could interfere with the activation and proliferation of SCs with the subsequent impairment of myofiber regeneration and muscle remodelling in sarcopenia.^{160,162} In this regard, it should be expected that the reduction in the proportion of SCs we found in old muscles negatively affects the regenerative capacity of muscles and exacerbates muscle fibrosis.^{163,164} Connective tissue deposition was found in all muscles from old mice, although it was particularly conspicuous in the EDL and Sol. Although the fibrotic tissue deposition would contribute to worsen the impaired muscle function in ageing, fibrosis could explain the absence of significant age-related changes in the muscle weight we observed in EDL and Sol muscles despite myofiber loss.

Interestingly, compared with adult mice, no statistically significant differences in muscle mass were found in old muscles, although in the latter, some decrease in the average weight was observed in Sol and EDL muscles. Overall, these findings suggest that ageing has only a minor impact on muscle mass of mice, a result which contrasts with reported data from human studies but is in agreement with previous analysis conducted in ageing rats and mice: in these models, only moderate or very small decreases in muscle mass have been observed compared with humans (reviewed by Ballak *et al.*⁹⁹). Moreover, the fact that Sol and EDL muscles, two distal hindlimb muscles with different fibre type composition, have a greater tendency for age-related mass reduction than the distal TA or the proximal Gra muscles corroborates the hypothesis that different muscles are impacted by varying degrees over the ageing process. This may suggest that muscle wasting in advanced ages could be more linked to both muscle location and specific function than to fibre type composition. In fact, others have reported differences in age-related muscle mass loss between mouse hindlimb (Sol and EDL) and the cervical (sternomastoid and cleidomastoid) muscles, with no changes in the latter.¹⁶⁵ In addition, it has been shown in rats¹⁶⁶ and also in humans¹⁶⁷ that hindlimb (leg) muscles are more severely affected than forelimb (arm) muscles. Our results indicate that even muscles in proximity of each other, such as TA and EDL, also display differential age-related histological alterations, with a significant decrease in fibre density in the EDL muscle and no overt changes in the TA muscle of old animals. These observations are somehow surprising because EDL and TA muscles have a similar fibre type composition and belong to the same functional group, and, consequently, we should expect

comparable age-associated alterations in both muscles. These observations point to the fact that the specific function and the degree of activity of muscles could be main determinants of muscle wasting severity in elderly.

All the old muscles examined in our study displayed fibres having central nuclei, with much higher proportions of them in TA and Gra muscles. The existence of increased amounts of fibres with centrally located nuclei has been associated to different muscle disorders and repair.⁸⁸ In the case of muscle repair, the fusion of activated SCs with the damaged myofiber causes the incorporation of new nuclei, which move first to the centre of the myofiber before moving out to its periphery. Therefore, the presence of centrally positioned nuclei has been considered as an indicator of myofiber regeneration. In this regard, the finding of elevated numbers of fibres with central nuclei in old muscles might reflect a process of continual myofiber regeneration in response to a persistent muscular impairment occurring with ageing. Changes in the NMJs leading to denervation/reinnervation could be one of the main drivers of fibre degeneration/regeneration cycles in aged muscles. However, an intrinsic alteration in myofibers as a cause of muscle dysfunction in elderly cannot be excluded. Thus, nuclear misposition should be considered not only a sign of muscle pathology but also a cause of it.⁸⁸ In any case, the finding of myofibers with centrally positioned nuclei in all the old muscles, but at different proportions, suggests that myofiber regeneration in ageing is a general feature shared by distinct types of hindlimb muscles, although they exhibited a highly variable degree of repair. Interestingly, muscles with the lowest numbers of myofibers with central nuclei (EDL and Sol) also appeared to display the lowest capacity of myofiber regeneration: both these muscles from old animals, predominantly the EDL, exhibited a reduction in the density of myofibers, indicating that regeneration cannot fully counteract myofiber loss. In fact, we failed to detect any decline in the fibre density in the old TA and Gra muscles, which have the highest number of fibres displaying central nuclei.

Studies performed in rat models have reported that age-related changes in muscle innervation results in a decreased proportion of type 2 myofibers, and particularly of those having a glycolytic metabolism (type 2B)^{94,95} (see also McKinnon *et al.* and Schiaffino and Reggiani^{86,92} as reviews). Type 2 myofibers are innervated by fast, MMP-9-positive, vulnerable MNs.^{43,45} The age-related decrease in the proportion of type 2 myofibers appears to be compensated by the increased numbers of type 1 myofibers,^{94,95} which, innervated by slow MNs, have an oxidative metabolism and are more resistant to degeneration. In fact, several analyses conducted in models of MN diseases have reported that MNs and synapses innervating type 2B myofibers degenerate earlier than those innervating types 2A and 1 myofibers.^{168,169} These results have been correlated with differences in the degree of plasticity of synapses: synapses exhibiting a low sprouting competence are the most vulnerable, whereas those which react with a

robust sprouting are selectively resistant.¹⁶⁸ Thus, it has been proposed that fibre type 2 to 1 transition in ageing is the consequence of a preferential loss of fast, vulnerable, MNs with the resulting denervation of 2B fibres and their subsequent innervation by slow, resistant, MNs with high sprouting capacity. In fact, myofiber type 2 to type 1 switching has been reported to occur in models of MN diseases, such as SMA mice.^{39,170} Because skeletal muscles with a higher content of type 1 fibres are more resistant to wasting than those with a predominance of type 2 fibres,^{92,171} it has been proposed that fibre type 2 to type 1 transition in these diseases could result from the activation of metabolic oxidative myogenic compensatory programme aimed at limiting muscle dysfunction. Our results indicate that a similar mechanism does not likely operate in muscles of C57BL/6J mice with ageing. In divergence with data from ageing rat studies, with the exception of Gra muscle, we did not observe any significant augment in the proportion of fibre type 1 in old muscles. Conversely, a trend to an age-related decrease in the amount of type 1 fibres was seen in all the distal hindlimb muscles, this reduction being particularly prominent in the EDL muscle. Additionally, in the old slow-twitch Sol muscle, the proportion of type 2A fibres was found prominently increased at the expense of a reduction in the number of types 1 and 2B fibres. These results corroborate previous findings indicating that fibre type 2 to 1 switching in ageing is not a common feature shared by all muscles, with profound differences existing between fast-twitch and slow-twitch muscles.¹⁶⁵ Additionally, our data suggest that differences in aged-related myofiber type transition also occur between muscles having similar fibre type composition but different limb topography (i.e. the distal TA or EDL and the proximal Gra muscle; all of them are fast-twitch muscles). It is important to note that there is a substantial inconsistency between the age-related changes in fibre type composition reported in the literature. Some studies in human muscles have found a type 2 to type 1 fibre switching with a reduction in the former, whereas other analyses have conversely reported aged-related increases in type 2 fibres; other works, however, have found no changes in muscle-fibre type profiles in humans with ageing.^{172–175} Similar disparities in age-associated fibre type transitions have been found in rodent studies.^{165,176–178} The absence of a consistent pattern of fibre type alterations, we found in old muscles, correlates with the absence of substantial MN death and, more specifically, with the lack of a decline in the proportion of vulnerable (MMP-9-positive) MNs. Overall, our data suggest that fibre type changes are more of a consequence of MN dysfunction than cell death.

The accumulation of lipofuscin in postmitotic cells is widely considered a hallmark of ageing (reviewed by Brunk and Terman⁹⁶ and Gray and Woulfe⁹⁷). In this respect, the presence of lipofuscin granules in brain cells, particularly in cerebral cortex and motor areas, is one of the most consistent features of ageing.¹⁷⁹ In a recent study, the content of lipofuscin aggregates has been analysed in MNs of old mice

and rhesus monkeys as a marker of neuronal ageing.¹⁰⁰ In this work, authors have shown a variable degree of lipofuscin accumulation among MNs, suggesting that not all MNs aged either at a comparable rate or at the same time. In a similar way, we noticed that in sharp contrast with the absence of lipofuscin in adult muscles, all old muscles from C57BL/6J mice accumulate this pigment in the myofiber cytosol. We observed, however, remarkable variations in the amounts of lipofuscin between the different muscles examined, with the slow-twitch Sol muscle exhibiting the lowest proportion of the lipid pigment and the fast-twitch Gra muscle the highest. These differences correlate with the finding that the fast-twitch types 2A and 2B myofibers are those which exhibited the highest content of lipofuscin in old muscles, with type 1 fibres almost devoid of the pigment granules. This indicates that vulnerable (types 2A and 2B) fibres are more prone to ageing than type 1 fibres. Large numbers of lipofuscin granules have been reported to be present in different muscular dystrophies in humans and young dystrophin-deficient *mdx* mice.^{180–182} It has been proposed that cellular lipofuscin accumulation is the consequence of an oxidative stress process making cellular components undegradable by lysosomal enzymes.⁹⁶ Indeed, the treatment of young *mdx* mice with antioxidants reduces lipofuscin accumulation and improves muscle function. Oxidation, as a cause of lipofuscin formation, seems to be also linked to a decreased degradative capacity of lysosomes, which would occur with age or under pathological conditions. It is not clear, however, whether lipofuscin really interferes with normal cellular function or, conversely, the accumulation of this pigment is a mere result from a previous cellular disturbance. Several pieces of evidence suggest that a detrimental feedback loop leading to lysosomal and ubiquitin/proteasome pathway inhibition may occur as a result of lipofuscin aggregation. In any case, it seems plausible that the accumulated lipofuscin makes cells more vulnerable to pathologic stimuli and decreases the cellular adaptability and response capacity to injury.⁹⁶ In the case of aged MNs, lipofuscin accumulation does not associate with cell atrophy or death, although it appears to correlate with the unequivocal alterations occurring with ageing in motor nerve terminals.¹⁰⁰ Moreover, although the lipofuscin aggregation is significantly higher in muscle fibres with peripheral nuclei, the presence of a certain proportion of fibres with central nuclei indicates the existence of newly regenerated myofibers already containing the age pigment. Whether or not lipofuscin granules in these fibres correlates with an impaired cellular function already present in the initial steps of myogenic programme should be analysed.

In summary, ageing in mice is accompanied by defects in motor skills and changes in the electromyographic patterns. These alterations occur in the absence of significant MN death but are associated to prominent MN deafferentation and reactive gliosis, which possibly contributes to MN impairment. Therefore, age-related MN dysfunction rather than

death could be responsible of structural and molecular alterations in motor axons, MNJs, and skeletal muscles found in senescence. The ageing progress appears to entail continuous cycles of motor axon degeneration/regeneration and sprouting, as deduced by the signs of morphologically altered motor axons in adult mice and the increased numbers of clustered small myelinated axons found in VRs of middle-aged mice. Although the distinct types of old muscles examined share some common features indicative of the ageing process, the profile of some alterations is markedly variable between muscles. This variability exists even between muscles located in close vicinity and having similar fibre type composition, suggesting that the degree of activity and specific function of muscles, rather than their topography and fibre typology, has greater impact on age-related muscular changes. Further research is needed to draw more reliable conclusions concerning the pathogenic mechanisms underlying neuromuscular alterations during ageing and the extent of their contribution to development of sarcopenia.

Funding

This work was supported by Abbott and a grant from the *Ministerio de Ciencia, Innovación y Universidades* cofinanced by *Fondo Europeo de Desarrollo Regional* (RTI2018-099278-B-I00 to J.C. and J.E.).

Author contributions

J.C., J.E.E., S.L.P., A.Ba., T.D., and R.R. contributed to conception of the research, and J.C. and J.E.E. designed the study. A. B., S.G., G.M.-C., O.T., A.C., and L.P. performed the research. A.B., S.G., O.T., X.N., and J.C. analysed the data. J.C., J.E.E., X. N., and S.L.P. contributed to writing the paper.

Acknowledgements

We thank Sara Salvany, Sara Hernández, Alaó Gatiús, Mònica Esteve, Maria Beltrán, and Clara Paniagua for collaborating in some experiments, Anaïs Panosa from the SCT of Microscopy of the *Universitat de Lleida* for technical support with confocal microscopy, and the staff from the SCT Animal Facility of the *Universitat de Lleida* for mouse care and housing. The authors certify that they comply with the ethical guidelines for

authorship and publishing in the *Journal of Cachexia, Sarcopenia and Muscle*.¹⁸³

Online supplementary material

Additional supporting information may be found online in the Supporting Information section at the end of the article.

Figure S1. Aging is accompanied by a decline in body weight and motor performance measured with the open-field test. **A)** Body weight in adult (4–10 months) and old (19–28 months) mice; *** $p < 0.001$ vs. adult 46 weeks. **B and C)** Motor performance assessed by open-field test in mice from 24 months of age on; the distance (in cm, **B**) and average speed (cm/s, **C**) in the course of the 16 week-period in which measurements were performed. * $p < 0.05$, ** $p < 0.01$, and *** $p < 0.001$ vs. 0 weeks. Data in the graphs are shown as the mean \pm SEM, $n = 15$ (84 to 112 weeks); $n = 8$ (~116 weeks onwards).

Figure S2. Age-related changes in DRG sensory neurons. **A-C, F-H and K-M)** Proportion (**A, F, K**) and soma area (**B, G, L**) of sensory neurons expressing CGRP (**A, B**), IB4 (**F, G**) and PV (**K, L**) in DRGs. **C, H, M)** Relative size-frequency (expressed as soma area in μm^2) histogram of DRG neurons showing CGRP- (**C**), IB4- (**H**) and PV- (**M**) positive staining. **D1-O2)** Representative micrographs taken from DRG cryostat sections processed for CGRP, IB4 and PV staining (green), as indicated. Sections were also counterstained with fluorescent Nissl (red) for neuron visualization. Data in the graphs are expressed as the mean \pm SEM, ** $p < 0.01$ and *** $p < 0.001$ vs. adult; $n = 4$ ventral roots of different animals per age group (Student's t -test). Scale bar: in **O2** = $100 \mu\text{m}^2$ (valid for **D1-E2, I1-J2** and **N1-O1**).

Conflict of interest

A.Ba., S.L.P., T.D., and R.R. are employees of Abbott. The other authors declare that they have no conflict of interest.

References

1. Fried LP, Tangen CM, Walston J, Newman AB, Hirsch C, Gottdiener J, et al. Frailty in older adults: evidence for a phenotype. *J Gerontol A Biol Sci Med Sci* 2001;**56**: M146–M156.
2. Cardoso AL, Fernandes A, Aguilar-Pimentel JA, de Angelis MH, Guedes JR, Brito MA, et al. Towards frailty biomarkers: candidates from genes and pathways regulated in aging and age-related diseases. *Ageing Res Rev* 2018;**47**:214–277.
3. Janssen I, Baumgartner RN, Ross R, Rosenberg IH, Roubenoff R. Skeletal muscle cutpoints associated with elevated

- physical disability risk in older men and women. *Am J Epidemiol* 2004;**159**:413–421.
4. Abellan van Kan G. Epidemiology and consequences of sarcopenia. *J Nutr Health Aging* 2009;**13**:708–712.
 5. von Haehling S, Morley JE, Anker SD. An overview of sarcopenia: facts and numbers on prevalence and clinical impact. *J Cachexia Sarcopenia Muscle* 2010;**1**:129–133.
 6. Larsson L, Degens H, Li M, Salvati L, Lee YI, Thompson W, et al. Sarcopenia: aging-related loss of muscle mass and function. *Physiol Rev* 2019;**99**:427–511.
 7. Kalinkovich A, Livshits G. Sarcopenia—the search for emerging biomarkers. *Ageing Res Rev* 2015;**22**:58–71.
 8. Berger MJ, Doherty TJ. Sarcopenia: prevalence, mechanisms, and functional consequences. *Interdiscip Top Gerontol* 2010;**37**:94–114.
 9. Rowan SL, Rygiel K, Purves-Smith FM, Solbak NM, Turnbull DM, Hepple RT. Denervation causes fiber atrophy and myosin heavy chain co-expression in senescent skeletal muscle. *PLoS ONE* 2012;**7**:e29082.
 10. Khosa S, Trikamji B, Khosa GS, Khanli HM, Mishra SK. An overview of neuromuscular junction aging findings in human and animal studies. *Curr Aging Sci* 2019;**12**:28–34.
 11. Willadt S, Nash M, Slater C. Age-related changes in the structure and function of mammalian neuromuscular junctions. *Ann N Y Acad Sci* 2018;**1412**:41–53.
 12. Jang YC, Van Remmen H. Age-associated alterations of the neuromuscular junction. *Exp Gerontol* 2011;**46**:193–198.
 13. Kang H, Lichtman JW. Motor axon regeneration and muscle reinnervation in young adult and aged animals. *J Neurosci* 2013;**33**:19480–19491.
 14. Tomlinson BE, Irving D. The numbers of limb motor neurons in the human lumbosacral cord throughout life. *J Neurol Sci* 1977;**34**:213–219.
 15. Ishihara A, Naitoh H, Katsuta S. Effects of ageing on the total number of muscle fibers and motoneurons of the tibialis anterior and soleus muscles in the rat. *Brain Res* 1987;**435**:355–358.
 16. Hashizume K, Kanda K. Neuronal dropout is greater in hindlimb motor nuclei than in forelimb motor nuclei in aged rats. *Neurosci Lett* 1990;**113**:267–269.
 17. Jacob JM. Lumbar motor neuron size and number is affected by age in male F344 rats. *Mech Ageing Dev* 1998;**106**:205–216.
 18. Doherty TJ, Vandervoort AA, Brown WF. Effects of ageing on the motor unit: a brief review. *Can J Appl Physiol = Revue canadienne de physiologie appliquee* 1993;**18**:331–358.
 19. Power GA, Dalton BH, Behm DG, Vandervoort AA, Doherty TJ, Rice CL. Motor unit number estimates in masters runners: use it or lose it? *Med Sci Sports Exerc* 2010;**42**:1644–1650.
 20. McKinnon NB, Montero-Odasso M, Doherty TJ. Motor unit loss is accompanied by decreased peak muscle power in the lower limb of older adults. *Exp Gerontol* 2015;**70**:111–118.
 21. Chopek JW, Gardiner PF. Life-long caloric restriction: effect on age-related changes in motoneuron numbers, sizes and apoptotic markers. *Mech Ageing Dev* 2010;**131**:650–659.
 22. Chai RJ, Vukovic J, Dunlop S, Grounds MD, Shavlakadze T. Striking denervation of neuromuscular junctions without lumbar motoneuron loss in geriatric mouse muscle. *PLoS ONE* 2011;**6**:e28090.
 23. Gonzalez M, Ruggiero FP, Chang Q, Shi YJ, Rich MM, Kraner S, et al. Disruption of TrkB-mediated signaling induces disassembly of postsynaptic receptor clusters at neuromuscular junctions. *Neuron* 1999;**24**:567–583.
 24. Funakoshi H, Belluardo N, Arenas E, Yamamoto Y, Casabona A, Persson H, et al. Muscle-derived neurotrophin-4 as an activity-dependent trophic signal for adult motor-neurons. *Science* 1995;**268**:1495–1499.
 25. Schinder AF, Poo M. The neurotrophin hypothesis for synaptic plasticity. *Trends Neurosci* 2000;**23**:639–645.
 26. Messi ML, Delbono O. Target-derived trophic effect on skeletal muscle innervation in senescent mice. *J Neurosci* 2003;**23**:1351–1359.
 27. Belluardo N, Westerblad H, Mudo G, Casabona A, Bruton J, Caniglia G, et al. Neuromuscular junction disassembly and muscle fatigue in mice lacking neurotrophin-4. *Mol Cell Neurosci* 2001;**18**:56–67.
 28. Jones RA, Harrison C, Eaton SL, Llaverro Hurtado M, Graham LC, Alkhamash L, et al. Cellular and molecular anatomy of the human neuromuscular junction. *Cell Rep* 2017;**21**:2348–2356.
 29. Flurkey K, Currer JM, Harrison DE, In Fox JG, Davisson MT, Quimby FW, Barthold SW, Newcomer CE, Smith AL, eds. *The Mouse in Biomedical Research Normative Biology, Husbandry, and Models*, 2nd ed. New York: Elsevier; 2007. p 637–672.
 30. Miller RA, Nadon NL. Principles of animal use for gerontological research. *J Gerontol a-Biol* 2000;**55**:B117–B123.
 31. Burkholder T, Foltz C, Karlsson E, Linton CG, Smith JM. Health evaluation of experimental laboratory mice. *Curr Protocols Mouse Biol* 2012;**2**:145–165.
 32. Brooks SP, Dunnett SB. Tests to assess motor phenotype in mice: a user's guide. *Nat Rev Neurosci* 2009;**10**:519–529.
 33. Navarro X, Udina E, Ceballos D, Gold BG. Effects of FK506 on nerve regeneration and reinnervation after graft or tube repair of long nerve gaps. *Muscle Nerve* 2001;**24**:905–915.
 34. Mancuso R, Santos-Nogueira E, Osta R, Navarro X. Electrophysiological analysis of a murine model of motoneuron disease. *Clin Neurophysiol* 2011;**122**:1660–1670.
 35. Bonetto A, Andersson DC, Waning DL. Assessment of muscle mass and strength in mice. *BoneKey Rep* 2015;**4**:732.
 36. Hebel R, Stromberg MW. *Myology. Anatomy of the Laboratory Rat*. Baltimore, U.S.A: Williams & Wilkins Company; 1976. p 18–42.
 37. Clarke PG, Oppenheim RW. Neuron death in vertebrate development: in vitro methods. *Methods Cell Biol* 1995;**46**:277–321.
 38. Calderó J, Ciutat D, Lladó J, Castán E, Oppenheim RW, Esquerda JE. Effects of excitatory amino acids on neuromuscular development in the chick embryo. *J Comp Neurol* 1997;**387**:73–95.
 39. Cerveró C, Montull N, Tarabal O, Piedrafita L, Esquerda JE, Calderó J. Chronic treatment with the AMPK agonist AICAR prevents skeletal muscle pathology but fails to improve clinical outcome in a mouse model of severe spinal muscular atrophy. *Neurotherapeutics: the journal of the American Society for Experimental NeuroTherapeutics* 2016;**13**:198–216.
 40. Young K, Morrison H. Quantifying microglia morphology from photomicrographs of immunohistochemistry prepared tissue using ImageJ. *J Visual Exp: JoVE* 2018;**136**.
 41. Kawamura Y, O'Brien P, Okazaki H, Dyck PJ. Lumbar motoneurons of man II: the number and diameter distribution of large- and intermediate-diameter cytons in 'motoneuron columns' of spinal cord of man. *J Neuropathol Exp Neurol* 1977;**36**:861–870.
 42. Sugiura M, Kanda K. Progress of age-related changes in properties of motor units in the gastrocnemius muscle of rats. *J Neurophysiol* 2004;**92**:1357–1365.
 43. Nijssen J, Comley LH, Hedlund E. Motor neuron vulnerability and resistance in amyotrophic lateral sclerosis. *Acta Neuropathol* 2017;**133**:863–885.
 44. Pun S, Santos AF, Saxena S, Xu L, Caroni P. Selective vulnerability and pruning of phasic motoneuron axons in motoneuron disease alleviated by CNTF. *Nat Neurosci* 2006;**9**:408–419.
 45. Kaplan A, Spiller KJ, Towne C, Kanning KC, Choe GT, Geber A, et al. Neuronal matrix metalloproteinase-9 is a determinant of selective neurodegeneration. *Neuron* 2014;**81**:333–348.
 46. New HV, Mudge AW. Calcitonin gene-related peptide regulates muscle acetylcholine receptor synthesis. *Nature* 1986;**323**:809–811.
 47. Sala C, Andreose JS, Fumagalli G, Lomo T. Calcitonin gene-related peptide: possible role in formation and maintenance of neuromuscular junctions. *J Neurosci* 1995;**15**:520–528.
 48. Matteoli M, Haimann C, Torritarelli F, Polak JM, Ceccarelli B, Decamilli P. Differential effect of alpha-latrotoxin on exocytosis from small synaptic vesicles and from large dense-core vesicles containing calcitonin gene-related peptide at the frog neuromuscular junction. *P Natl Acad Sci USA* 1988;**85**:7366–7370.

49. Calderó J, Casanovas A, Sorribas A, Esquerda JE. Calcitonin gene-related peptide in rat spinal cord motoneurons: subcellular distribution and changes induced by axotomy. *Neuroscience* 1992;**48**:449–461.
50. Tarabal O, Calderó J, Ribera J, Sorribas A, López R, Molgó J, et al. Regulation of motoneuronal calcitonin gene-related peptide (CGRP) during axonal growth and neuromuscular synaptic plasticity induced by botulinum toxin in rats. *Eur J Neurosci* 1996;**8**:829–836.
51. Piehl F, Arvidsson U, Johnson H, Cullheim S, Villar M, Dagerlind A, et al. Calcitonin gene-related peptide (CGRP)-like immunoreactivity and CGRP mRNA in rat spinal cord motoneurons after different types of lesions. *Eur J Neurosci* 1991;**3**:737–757.
52. Matteoli M, Balbi S, Sala C, Chini B, Cimino M, Vitadello M, et al. Developmentally regulated expression of calcitonin gene-related peptide at mammalian neuromuscular junction. *J Mol Neurosci* 1990;**2**:175–184.
53. Liddel SA, Barres BA. Reactive astrocytes: production, function, and therapeutic potential. *Immunity* 2017;**46**:957–967.
54. Aldskogius H, Kozlova EN. Central neuron–glial and glial–glial interactions following axon injury. *Prog Neurobiol* 1998;**55**:1–26.
55. Blackburn D, Sargsyan S, Monk PN, Shaw PJ. Astrocyte function and role in motor neuron disease: a future therapeutic target? *Glia* 2009;**57**:1251–1264.
56. Phillips T, Robberecht W. Neuroinflammation in amyotrophic lateral sclerosis: role of glial activation in motor neuron disease. *Lancet Neurol* 2011;**10**:253–263.
57. Salvany S, Casanovas A, Tarabal O, Piedrafita L, Hernandez S, Santafe M, et al. Localization and dynamic changes of neuregulin-1 at C-type synaptic boutons in association with motor neuron injury and repair. *FASEB J: official publication of the Federation of American Societies for Experimental Biology* 2019;**33**:7833–7851.
58. Tang Y, Le W. Differential roles of M1 and M2 microglia in neurodegenerative diseases. *Mol Neurobiol* 2016;**53**:1181–1194.
59. Kigerl KA, Gensel JC, Ankeny DP, Alexander JK, Donnelly DJ, Popovich PG. Identification of two distinct macrophage subsets with divergent effects causing either neurotoxicity or regeneration in the injured mouse spinal cord. *J Neurosci* 2009;**29**:13435–13444.
60. Franco R, Fernandez-Suarez D. Alternatively activated microglia and macrophages in the central nervous system. *Prog Neurobiol* 2015;**131**:65–86.
61. Liddel SA, Gattenplan KA, Clarke LE, Bennett FC, Bohlen CJ, Schirmer L, et al. Neurotoxic reactive astrocytes are induced by activated microglia. *Nature* 2017;**541**:481–487.
62. Kawamoto Y, Akiguchi I, Tomimoto H, Shirakashi Y, Honjo Y, Budka H. Upregulated expression of 14-3-3 proteins in astrocytes from human cerebrovascular ischemic lesions. *Stroke* 2006;**37**:830–835.
63. Conforti L, Gilley J, Coleman MP. Wallerian degeneration: an emerging axon death pathway linking injury and disease. *Nat Rev Neurosci* 2014;**15**:394–409.
64. Antal M, Freund TF, Polgar E. Calcium-binding proteins, parvalbumin- and calbindin-D 28k-immunoreactive neurons in the rat spinal cord and dorsal root ganglia: a light and electron microscopic study. *J Comp Neurol* 1990;**295**:467–484.
65. Fang X, Djouhri L, McMullan S, Berry C, Waxman SG, Okuse K, et al. Intense isolectin-B4 binding in rat dorsal root ganglion neurons distinguishes C-fiber nociceptors with broad action potentials and high Nav1.9 expression. *J Neurosci* 2006;**26**:7281–7292.
66. Marmigère F, Ernfors P. Specification and connectivity of neuronal subtypes in the sensory lineage. *Nat Rev Neurosci* 2007;**8**:114–127.
67. Valdez G, Tapia JC, Kang H, Clemenson GD Jr, Gage FH, Lichtman JW, et al. Attenuation of age-related changes in mouse neuromuscular synapses by caloric restriction and exercise. *Proc Natl Acad Sci U S A* 2010;**107**:14863–14868.
68. Valdez G, Tapia JC, Lichtman JW, Fox MA, Sanes JR. Shared resistance to aging and ALS in neuromuscular junctions of specific muscles. *PLoS ONE* 2012;**7**:e34640.
69. Willadt S, Nash M, Slater CR. Age-related fragmentation of the motor endplate is not associated with impaired neuromuscular transmission in the mouse diaphragm. *Sci Rep* 2016;**6**:24849.
70. Tarabal O, Calderó J, Esquerda JE. Intramuscular nerve sprouting induced by CNTF is associated with increases in CGRP content in mouse motor nerve terminals. *Neurosci Lett* 1996;**219**:60–64.
71. Holahan MR. A shift from a pivotal to supporting role for the growth-associated protein (GAP-43) in the coordination of axonal structural and functional plasticity. *Front Cell Neurosci* 2017;**11**:266.
72. Caroni P, Becker M. The downregulation of growth-associated proteins in motoneurons at the onset of synapse elimination is controlled by muscle activity and IGF1. *J Neurosci* 1992;**12**:3849–3861.
73. Li L, Xiong WC, Mei L. Neuromuscular junction formation, aging, and disorders. *Annu Rev Physiol* 2018;**80**:159–188.
74. Tintignac LA, Brenner HR, Ruegg MA. Mechanisms regulating neuromuscular junction development and function and causes of muscle wasting. *Physiol Rev* 2015;**95**:809–852.
75. Samuel MA, Valdez G, Tapia JC, Lichtman JW, Sanes JR. Agrin and synaptic laminin are required to maintain adult neuromuscular junctions. *PLoS ONE* 2012;**7**:e46663.
76. Reist NE, Magill C, McMahan UJ. Agrin-like molecules at synaptic sites in normal, denervated, and damaged skeletal muscles. *J Cell Biol* 1987;**105**:2457–2469.
77. Tassi E, Al-Attar A, Aigner A, Swift MR, McDonnell K, Karavanov A, et al. Enhancement of fibroblast growth factor (FGF) activity by an FGF-binding protein. *J Biol Chem* 2001;**276**:40247–40253.
78. Williams AH, Valdez G, Moresi V, Qi X, McAnally J, Elliott JL, et al. MicroRNA-206 delays ALS progression and promotes regeneration of neuromuscular synapses in mice. *Science* 2009;**326**:1549–1554.
79. Taetzsch T, Tenga MJ, Valdez G. Muscle fibers secrete FGFBP1 to slow degeneration of neuromuscular synapses during aging and progression of ALS. *J Neurosci: the official journal of the Society for Neuroscience* 2017;**37**:70–82.
80. Faitg J, Leduc-Gaudet JP, Reynaud O, Ferland G, Gaudreau P, Gouspillou G. Effects of aging and caloric restriction on fiber type composition, mitochondrial morphology and dynamics in rat oxidative and glycolytic muscles. *Front Physiol* 2019;**10**:420.
81. Ascenzi F, Barberi L, Dobrowolny G, Villa Nova Bacurau A, Nicoletti C, Rizzuto E, et al. Effects of IGF-1 isoforms on muscle growth and sarcopenia. *Aging Cell* 2019;**18**:e12954.
82. Chung T, Park JS, Kim S, Montes N, Walston J, Hoke A. Evidence for dying-back axonal degeneration in age-associated skeletal muscle decline. *Muscle Nerve* 2017;**55**:894–901.
83. Brooks SV, Faulkner JA. Contractile properties of skeletal muscles from young, adult and aged mice. *J Physiol* 1988;**404**:71–82.
84. Caccia MR, Harris JB, Johnson MA. Morphology and physiology of skeletal muscle in aging rodents. *Muscle Nerve* 1979;**2**:202–212.
85. Hunter SK, Pereira HM, Keenan KG. The aging neuromuscular system and motor performance. *J Appl Physiol* 2016;**121**:982–995.
86. McKinnon NB, Connelly DM, Rice CL, Hunter SW, Doherty TJ. Neuromuscular contributions to the age-related reduction in muscle power: mechanisms and potential role of high velocity power training. *Ageing Res Rev* 2017;**35**:147–154.
87. Carlson BM. The regeneration of skeletal muscle. A review. *Am J Anat* 1973;**137**:119–149.
88. Folker ES, Bayliss MK. Nuclear positioning in muscle development and disease. *Front Physiol* 2013;**4**:363.
89. Sacco A, Puri PL. Regulation of muscle satellite cell function in tissue homeostasis and aging. *Cell Stem Cell* 2015;**16**:585–587.
90. Sousa-Victor P, García-Prat L, Serrano AL, Perdiguero E, Muñoz-Cánoves P. Muscle stem cell aging: regulation and rejuvenation. *Trends Endocrinol Metab: TEM* 2015;**26**:287–296.
91. Pette D, Staron RS. Myosin isoforms, muscle fiber types, and transitions. *Microsc Res Tech* 2000;**50**:500–509.
92. Schiaffino S, Reggiani C. Fiber types in mammalian skeletal muscles. *Physiol Rev* 2011;**91**:1447–1531.

93. Hamalainen N, Pette D. The histochemical profiles of fast fiber types IIB, IID, and IIA in skeletal muscles of mouse, rat, and rabbit. *J Histochem Cytochem: official journal of the Histochemistry Society* 1993;**41**:733–743.
94. Larsson L, Edstrom L, Lindegren B, Gorza L, Schiaffino S. MHC composition and enzyme-histochemical and physiological properties of a novel fast-twitch motor unit type. *Am J Physiol* 1991;**261**:C93–C101.
95. Larsson L, Biral D, Campione M, Schiaffino S. An age-related type IIB to IIX myosin heavy chain switching in rat skeletal muscle. *Acta Physiol Scand* 1993;**147**:227–234.
96. Brunk UT, Terman A. Lipofuscin: mechanisms of age-related accumulation and influence on cell function. 12 Guest Editor: Rajindar S. Sohal. This article is part of a series of reviews on “Oxidative Stress and Aging.” The full list of papers may be found on the homepage of the journal. *Free Radic Biol Med* 2002;**33**:611–619.
97. Gray DA, Woulfe J. Lipofuscin and aging: a matter of toxic waste. *Sci Aging Knowledge Environ*: SAGE KE 2005;**2005**:re1.
98. Terman A, Abrahamsson N, Brunk UT. Ceroid/lipofuscin-loaded human fibroblasts show increased susceptibility to oxidative stress. *Exp Gerontol* 1999;**34**:755–770.
99. Ballak SB, Degens H, de Haan A, Jaspers RT. Aging related changes in determinants of muscle force generating capacity: a comparison of muscle aging in men and male rodents. *Ageing Res Rev* 2014;**14**:43–55.
100. Maxwell N, Castro RW, Sutherland NM, Vaughan KL, Szarowicz MD, de Cabo R, et al. α -Motor neurons are spared from aging while their synaptic inputs degenerate in monkeys and mice. *Aging Cell* 2018;**17**:e12726.
101. Calderó J, Prevette D, Mei X, Oakley RA, Li L, Milligan C, et al. Peripheral target regulation of the development and survival of spinal sensory and motor neurons in the chick embryo. *J Neurosci* 1998;**18**:356–370.
102. Zimatkin SM, Bon’ EI. Dark neurons of the brain. *Neurosci Behav Physiol* 2018;**48**:908–912.
103. Gallyas F. Novel cell-biological ideas deducible from morphological observations on ‘dark’ neurons revisited. *Idegyogy Sz* 2007;**60**:212–222.
104. Ooigawa H, Nawashiro H, Fukui S, Otani N, Osumi A, Toyooka T, et al. The fate of Nissl-stained dark neurons following traumatic brain injury in rats: difference between neocortex and hippocampus regarding survival rate. *Acta Neuropathol* 2006;**112**:471–481.
105. Kovesdi E, Pal J, Gallyas F. The fate of ‘dark’ neurons produced by transient focal cerebral ischemia in a non-necrotic and non-excitotoxic environment: neurobiological aspects. *Brain Res* 2007;**1147**:272–283.
106. Krishnan VS, Shavliakadze T, Grounds MD, Hodgetts SI, Harvey AR. Age-related loss of VGLUT1 excitatory, but not VGAT inhibitory, immunoreactive terminals on motor neurons in spinal cords of old sarcopenic male mice. *Biogerontology* 2018;**19**:385–399.
107. Cerveró C, Blasco A, Tarabal O, Casanovas A, Piedrafita L, Navarro X, et al. Glial activation and central synapse loss, but not motoneuron degeneration, are prevented by the sigma-1 receptor agonist PRE-084 in the Smn2B^{-/-} mouse model of spinal muscular atrophy. *J Neuropathol Exp Neurol* 2018;**77**:577–597.
108. Tarabal O, Caraballo-Miralles V, Cardona-Rossinyol A, Correa FJ, Olmos G, Lladó J, et al. Mechanisms involved in spinal cord central synapse loss in a mouse model of spinal muscular atrophy. *J Neuropathol Exp Neurol* 2014;**73**:519–535.
109. Gallart-Palau X, Tarabal O, Casanovas A, Sábado J, Correa FJ, Hereu M, et al. Neuregulin-1 is concentrated in the post-synaptic subsurface cistern of C-bouton inputs to α -motoneurons and altered during motoneuron diseases. *FASEB J* 2014;**28**:3618–3632.
110. Ling KK, Lin MY, Zingg B, Feng Z, Ko CP. Synaptic defects in the spinal and neuromuscular circuitry in a mouse model of spinal muscular atrophy. *PLoS ONE* 2010;**5**:e15457.
111. Mentis GZ, Blivis D, Liu W, Drobac E, Crowder ME, Kong L, et al. Early functional impairment of sensory-motor connectivity in a mouse model of spinal muscular atrophy. *Neuron* 2011;**69**:453–467.
112. Milan L, Courtand G, Carroit L, Masmejean F, Barriere G, Cazalets JR, et al. Age-related changes in pre- and postsynaptic partners of the cholinergic C-boutons in wild-type and SOD1G93A lumbar motoneurons. *PLoS ONE* 2015;**10**:e0135525.
113. Saxena S, Roselli F, Singh K, Leptien K, Julien JP, Gros-Louis F, et al. Neuroprotection through excitability and mTOR required in ALS motoneurons to delay disease and extend survival. *Neuron* 2013;**80**:80–96.
114. Pullen AH, Athanasiou D. Increase in pre-synaptic territory of C-terminals on lumbar motoneurons of G93A SOD1 mice during disease progression. *Eur J Neurosci* 2009;**29**:551–561.
115. Sunico CR, Dominguez G, Garcia-Verdugo JM, Osta R, Montero F, Moreno-Lopez B. Reduction in the motoneuron inhibitory/excitatory synaptic ratio in an early-symptomatic mouse model of amyotrophic lateral sclerosis. *Brain Pathol* 2011;**21**:1–15.
116. Alvarez FJ, Titus-Mitchell HE, Bullinger KL, Kraszpulski M, Nardelli P, Cope TC. Permanent central synaptic disconnection of proprioceptors after nerve injury and regeneration. I. Loss of VGLUT1/IA synapses on motoneurons. *J Neurophysiol* 2011;**106**:2450–2470.
117. Rotterman TM, Nardelli P, Cope TC, Alvarez FJ. Normal distribution of VGLUT1 synapses on spinal motoneuron dendrites and their reorganization after nerve injury. *J Neurosci* 2014;**34**:3475–3492.
118. Rekling JC, Funk GD, Bayliss DA, Dong XW, Feldman JL. Synaptic control of motoneuronal excitability. *Physiol Rev* 2000;**80**:767–852.
119. Rodríguez-Arellano JJ, Parpura V, Zorec R, Verkhatsky A. Astrocytes in physiological aging and Alzheimer’s disease. *Neuroscience* 2016;**323**:170–182.
120. Spittau B. Aging microglia-phenotypes, functions and implications for age-related neurodegenerative diseases. *Front Aging Neurosci* 2017;**9**.
121. Wong WT. Microglial aging in the healthy CNS: phenotypes, drivers, and rejuvenation. *Front Cell Neurosci* 2013;**7**:22.
122. Evans MC, Couch Y, Sibson N, Turner MR. Inflammation and neurovascular changes in amyotrophic lateral sclerosis. *Mol Cell Neurosci* 2013;**53**:34–41.
123. McGivern JV, Patitucci TN, Nord JA, Barabas MA, Stucky CL, Ebert AD. Spinal muscular atrophy astrocytes exhibit abnormal calcium regulation and reduced growth factor production. *Glia* 2013;**61**:1418–1428.
124. Papadimitriou D, Le Verche V, Jacquier A, Ikiz B, Przedborski S, Re DB. Inflammation in ALS and SMA: sorting out the good from the evil. *Neurobiol Dis* 2010;**37**:493–502.
125. Giorgetti E, Panesar M, Zhang Y, Joller S, Ronco M, Obrecht M, et al. Modulation of microglia by voluntary exercise or CSF1R inhibition prevents age-related loss of functional motor units. *Cell Rep* 2019;**29**:1539–1554 e7.
126. Henstridge CM, Tzioras M, Paolicelli RC. Glial contribution to excitatory and inhibitory synapse loss in neurodegeneration. *Front Cell Neurosci* 2019;**13**:63.
127. Chung WS, Clarke LE, Wang GX, Stafford BK, Sher A, Chakraborty C, et al. Astrocytes mediate synapse elimination through MEGF10 and MERTK pathways. *Nature* 2013;**504**:394–400.
128. Acharjee S, Verbeek M, Gomez CD, Bisht K, Lee B, Benoit L, et al. Reduced microglial activity and enhanced glutamate transmission in the basolateral amygdala in early CNS autoimmunity. *J Neurosci* 2018;**38**:9019–9033.
129. Wake H, Moorhouse AJ, Jinno S, Kohsaka S, Nabekura J. Resting microglia directly monitor the functional state of synapses in vivo and determine the fate of ischemic terminals. *J Neurosci* 2009;**29**:3974–3980.
130. Vaughan SK, Stanley OL, Valdez G. Impact of aging on proprioceptive sensory neurons and intrafusal muscle fibers in mice. *J Gerontol A Biol Sci Med Sci* 2017;**72**:771–779.
131. Chen HH, Hippenmeyer S, Arber S, Frank E. Development of the monosynaptic stretch reflex circuit. *Curr Opin Neurobiol* 2003;**13**:96–102.
132. Bulling DG, Kelly D, Bond S, McQueen DS, Seckl JR. Adjuvant-induced joint

- inflammation causes very rapid transcription of beta-preprotachykinin and alpha-CGRP genes in innervating sensory ganglia. *J Neurochem* 2001;**77**:372–382.
133. Mulder H, Zhang Y, Danielsen N, Sundler F. Islet amyloid polypeptide and calcitonin gene-related peptide expression are up-regulated in lumbar dorsal root ganglia after unilateral adjuvant-induced inflammation in the rat paw. *Mol Brain Res* 1997;**50**:127–135.
 134. Staton PC, Wilson AW, Bountra C, Chessell IP, Day NC. Changes in dorsal root ganglion CGRP expression in a chronic inflammatory model of the rat knee joint: differential modulation by rofecoxib and paracetamol. *Eur J Pain* 2007;**11**:283–289.
 135. Ohtori S, Takahashi K, Chiba T, Yamagata M, Sameda H, Moriya H. Phenotypic inflammation switch in rats shown by calcitonin gene-related peptide immunoreactive dorsal root ganglion neurons innervating the lumbar facet joints. *Spine* 2001;**26**:1009–1013.
 136. Navarro X, Udina E. Methods and protocols in peripheral nerve regeneration experimental research: part III-electrophysiological evaluation. *Int Rev Neurobiol* 2009;**87**:105–126.
 137. Sato A, Sato Y, Suzuki H. Aging effects on conduction velocities of myelinated and unmyelinated fibers of peripheral nerves. *Neurosci Lett* 1985;**53**:15–20.
 138. Schmelzer JD, Low PA. Electrophysiological studies on the effect of age on caudal nerve of the rat. *Exp Neurol* 1987;**96**:612–620.
 139. Verdú E, Buti M, Navarro X. Functional changes of the peripheral nervous system with aging in the mouse. *Neurobiol Aging* 1996;**17**:73–77.
 140. Buchthal F, Rosenfalck A, Behse F. Sensory potentials of normal and diseased nerves. In Dyck PJ, Thomas PK, Lambert EH, Bunge R, eds. *Peripheral Neuropathy*. Philadelphia: WB Saunders; 1984. p 981–1105.
 141. Dorfman LJ, Bosley TM. Age-related changes in peripheral and central nerve conduction in man. *Neurology* 1979;**29**:38–44.
 142. Taylor PK. Non-linear effects of age on nerve conduction in adults. *J Neurol Sci* 1984;**66**:223–234.
 143. Bouche P, Cattelín F, Saint-Jean O, Leger JM, Queslati S, Guez D, et al. Clinical and electrophysiological study of the peripheral nervous system in the elderly. *J Neurol* 1993;**240**:263–268.
 144. O'Sullivan DJ, Swallow M. The fibre size and content of the radial and sural nerves. *J Neurol Neurosurg Psychiatry* 1968;**31**:464–470.
 145. Sharma AK, Bajada S, Thomas PK. Age changes in the tibial and plantar nerves of the rat. *J Anat* 1980;**130**:417–428.
 146. Ceballos D, Cuadras J, Verdu E, Navarro X. Morphometric and ultrastructural changes with ageing in mouse peripheral nerve. *J Anat* 1999;**195**:563–576.
 147. Gawel M, Kostera-Pruszczyk A. Effect of age and gender on the number of motor units in healthy subjects estimated by the multipoint incremental MUNE method. *J Clin Neurophysiol: official publication of the American Electroencephalographic Society* 2014;**31**:272–278.
 148. Brown MC, Holland RL, Hopkins WG. Motor nerve sprouting. *Annu Rev Neurosci* 1981;**4**:17–42.
 149. Fagg GE, Scheff SW, Cotman CW. Axonal sprouting at the neuromuscular junction of adult and aged rats. *Exp Neurol* 1981;**74**:847–854.
 150. Jacob JM, Robbins N. Differential effects of age on neuromuscular transmission in partially sprouting mouse muscle. *J Neurosci* 1990;**10**:1522–1529.
 151. Fogarty MJ, Gonzalez Porras MA, Mantilla CB, Sieck GC. Diaphragm neuromuscular transmission failure in aged rats. *J Neurophysiol* 2019;**122**:93–104.
 152. Barker D, Ip MC. Sprouting and degeneration of mammalian motor axons in normal and de-afferented skeletal muscle. *Proc R Soc Lond B Biol Sci* 1966;**163**:538–554.
 153. Marques MJ, Conchello JA, Lichtman JW. From plaque to pretzel: fold formation and acetylcholine receptor loss at the developing neuromuscular junction. *J Neurosci* 2000;**20**:3663–3675.
 154. Li Y, Lee YI, Thompson WJ. Changes in aging mouse neuromuscular junctions are explained by degeneration and regeneration of muscle fiber segments at the synapse. *J Neurosci* 2011;**31**:14910–14919.
 155. Changeux JP, Duclert A, Sekine S. Calcitonin gene-related peptides and neuromuscular interactions. *Ann N Y Acad Sci* 1992;**657**:361–378.
 156. Chung AM. Calcitonin gene-related peptide (CGRP): role in peripheral nerve regeneration. *Rev Neurosci* 2018;**29**:369–376.
 157. Arvidsson U, Johnson H, Piehl F, Cullheim S, Hokfelt T, Risling M, et al. Peripheral nerve section induces increased levels of calcitonin gene-related peptide (CGRP)-like immunoreactivity in axotomized motoneurons. *Exp Brain Res* 1990;**79**:212–216.
 158. Haas CA, Streit WJ, Kreutzberg GW. Rat facial motoneurons express increased levels of calcitonin gene-related peptide mRNA in response to axotomy. *J Neurosci Res* 1990;**27**:270–275.
 159. Valsecchi V, Boido M, De Amicis E, Piras A, Vercelli A. Expression of muscle-specific MiRNA 206 in the progression of disease in a murine SMA model. *PLoS ONE* 2015;**10**:e0128560.
 160. Burks TN, Cohn RD. Role of TGF- β signaling in inherited and acquired myopathies. *Skeletal muscle* 2011;**1**:19.
 161. Serrano AL, Muñoz-Cánoves P. Regulation and dysregulation of fibrosis in skeletal muscle. *Exp Cell Res* 2010;**316**:3050–3058.
 162. Carlson ME, Conboy MJ, Hsu M, Barchas L, Jeong J, Agrawal A, et al. Relative roles of TGF- β 1 and Wnt in the systemic regulation and aging of satellite cell responses. *Aging Cell* 2009;**8**:676–689.
 163. Fry CS, Lee JD, Mula J, Kirby TJ, Jackson JR, Liu F, et al. Inducible depletion of satellite cells in adult, sedentary mice impairs muscle regenerative capacity without affecting sarcopenia. *Nat Med* 2015;**21**:76–80.
 164. Fry CS, Lee JD, Jackson JR, Kirby TJ, Stasko SA, Liu H, et al. Regulation of the muscle fiber microenvironment by activated satellite cells during hypertrophy. *FASEB J: Official publication of the Federation of American Societies for Experimental Biology* 2014;**28**:1654–1665.
 165. Sheard PW, Anderson RD. Age-related loss of muscle fibres is highly variable amongst mouse skeletal muscles. *Biogerontology* 2012;**13**:157–167.
 166. Hashizume K, Kanda K. Differential effects of aging on motoneurons and peripheral nerves innervating the hindlimb and forelimb muscles of rats. *Neurosci Res* 1995;**22**:189–196.
 167. Oertel G. Changes in human skeletal muscles due to ageing. Histological and histochemical observations on autopsy material. *Acta Neuropathol* 1986;**69**:309–313.
 168. Frey D, Schneider C, Xu L, Borg J, Spooren W, Caroni P. Early and selective loss of neuromuscular synapse subtypes with low sprouting competence in motoneuron diseases. *J Neurosci* 2000;**20**:2534–2542.
 169. Vinsant S, Mansfield C, Jimenez-Moreno R, Del Gaizo MV, Yoshikawa M, Hampton TG, et al. Characterization of early pathogenesis in the SOD1 (G93A) mouse model of ALS: part II, results and discussion. *Brain Behav* 2013;**3**:431–457.
 170. Lee YI, Mikesh M, Smith I, Rimer M, Thompson W. Muscles in a mouse model of spinal muscular atrophy show profound defects in neuromuscular development even in the absence of failure in neuromuscular transmission or loss of motor neurons. *Dev Biol* 2011;**356**:432–444.
 171. Minnaard R, Drost MR, Wagenmakers AJ, van Kranenburg GP, Kuipers H, Hesselink MK. Skeletal muscle wasting and contractile performance in septic rats. *Muscle Nerve* 2005;**31**:339–348.
 172. Frontera WR, Hughes VA, Fielding RA, Fiatarone MA, Evans WJ, Roubenoff R. Aging of skeletal muscle: a 12-yr longitudinal study. *J Appl Physiol* 2000;**88**:1321–1326.
 173. Lexell J, Taylor CC, Sjöström M. What is the cause of the ageing atrophy? *J Neurol Sci* 1988;**84**:275–294.
 174. Larsson L. Morphological and functional characteristics of the ageing skeletal muscle in man. A cross-sectional study. *Acta Physiol Scand Suppl* 1978;**457**:1–36.
 175. Hakkinen K, Newton RU, Gordon SE, McCormick M, Volek JS, Nindl BC, et al. Changes in muscle morphology, electromyographic activity, and force production characteristics during progressive strength training in young and older

- men. *J Gerontol A Biol Sci Med Sci* 1998;**53**:B415–B423.
176. Brown M, Hasser EM. Complexity of age-related change in skeletal muscle. *J Gerontol A Biol Sci Med Sci* 1996;**51**: B117–B123.
177. Carter EE, Thomas MM, Murynka T, Rowan SL, Wright KJ, Huba E, et al. Slow twitch soleus muscle is not protected from sarcopenia in senescent rats. *Exp Gerontol* 2010;**45**:662–670.
178. Deschenes MR, Roby MA, Eason MK, Harris MB. Remodeling of the neuromuscular junction precedes sarcopenia related alterations in myofibers. *Exp Gerontol* 2010;**45**:389–393.
179. Benavides SH, Monserrat AJ, Fariña S, Porta EA. Sequential histochemical studies of neuronal lipofuscin in human cerebral cortex from the first to the ninth decade of life. *Arch Gerontol Geriatr* 2002;**34**:219–231.
180. Nakae Y, Stoward PJ, Kashiwama T, Shono M, Akagi A, Matsuzaki T, et al. Early onset of lipofuscin accumulation in dystrophin-deficient skeletal muscles of DMD patients and *mdx* mice. *J Mol Histol* 2004;**35**:489–499.
181. Nakae Y, Stoward PJ. The high correlation between counts and area fractions of lipofuscin granules, a biomarker of oxidative stress in muscular dystrophies. *Histochem Cell Biol* 2016;**146**:627–634.
182. Terrill JR, Radley-Crabb HG, Iwasaki T, Lemckert FA, Arthur PG, Grounds MD. Oxidative stress and pathology in muscular dystrophies: focus on protein thiol oxidation and dysferlinopathies. *FEBS J* 2013;**280**:4149–4164.
183. von Haehling S, Morley JE, Coats AJS, Anker SD. Ethical guidelines for publishing in the *Journal of Cachexia, Sarcopenia and Muscle*: update 2019. *J Cachexia Sarcopenia Muscle* 2019;**10**:1143–1145.